

This PDF file is subject to the following conditions and restrictions:

Copyright © 2005, The Geological Society of America, Inc. (GSA). All rights reserved. Copyright not claimed on content prepared wholly by U.S. government employees within scope of their employment. Individual scientists are hereby granted permission, without fees or further requests to GSA, to use a single figure, a single table, and/or a brief paragraph of text in other subsequent works and to make unlimited copies for noncommercial use in classrooms to further education and science. For any other use, contact Copyright Permissions, GSA, P.O. Box 9140, Boulder, CO 80301-9140, USA, fax 303-357-1073, editing@geosociety.org. GSA provides this and other forums for the presentation of diverse opinions and positions by scientists worldwide, regardless of their race, citizenship, gender, religion, or political viewpoint. Opinions presented in this publication do not reflect official positions of the Society.

*An undeformed ophiolite in the Alps:
Field and geochemical evidence for a link between
volcanism and shallow plate tectonic processes*

Françoise Chalot-Prat*

CRPG-CNRS BP20, 15 rue Notre Dame des Pauvres 54501, Vandoeuvre Cedex, France

ABSTRACT

Detailed mapping and geochemistry of an undeformed Jurassic ophiolite (Chenaillet-Montgenèvre, Franco-Italian Alps) were performed to document the volcanic architecture at an axial ridge and its relationships with the chemical evolution of basalts and ocean spreading. The architecture of the volcanic cover resembles an abyssal hill with hummocky ridges and hundreds of hummocks, as described at the Atlantic axial volcanic ridge. Mantle rocks and gabbros, below and on both sides of the volcanic hill, are capped with cataclasite horizons representing detachment faults responsible for their exhumation on the seafloor. Basaltic cover and gabbro sills are thin. They overlie a dome-forming mantle basement, the undulated top of which is responsible for the relief variations.

Volcanoes formed on slopes, and the higher the edifice, the younger it is relative to the others. Two types of volcanic architecture, stairs and combs, exist. Stairs are associated with tongue-like volcanoes cascading down the steps. Combs consist of strings of conical volcanoes or hummocks, sitting at the intersections of major fissures parallel to the spreading axis, with oblique subsidiary fractures. Stairs emplaced by rifting of a basement in uplift and already denuded by detachment faulting. Combs formed on a basement in uplift and in the process of denudation along detachment faults serving as magma conduits at depth and as a conveyor belt for volcanoes on the sea floor to a limited extent (<500 m). In both cases, the magma chamber remained beneath the highest part of the relief. In the stairs and combs, rhythmic or continuous compositional variations occurred with time. They attest to cyclic eruptions of primary and differentiated melts, or to extraction of melts as they formed successively. The magma conduits were rooted in ephemeral, small, and frequently recharged reservoirs, or even in the mantle source. Lithospheric tectonics controlled not only magma ascent but also mantle melting.

Keywords: volcanic architecture, basalt geochemistry, mid-ocean ridge, lithospheric spreading, ophiolite

*E-mail: chalot@crpg.cnrs-nancy.fr.

INTRODUCTION

According to the standard plate tectonic theory, mid-ocean ridges are not sites of melting anomalies. Plate divergence is linked to upward mantle convection in the asthenosphere. This mantle convection leads to adiabatic decompression of the asthenosphere, partial melting, and magma extraction. The theory also assumes that the mantle is laterally isothermal and homogeneous. Spreading and magma genesis are interdependent, such that spreading without magma genesis is considered to be anomalous and to testify to a somewhat cold and/or infertile mantle (Meyzen et al., 2003, and references therein).

During the past 15 years, it has been reported that, whether on recent slow- to ultraslow-spreading ridges (Karson et al., 1987; Dick, 1989; Cannat, 1993; Cannat and Casey, 1995; Cannat et al., 1997) or on fast-spreading ridges (e.g., the western Pacific: Ohara et al., 2002, 2003), mantle peridotites outcrop at ridges on very large surfaces without any nearby gabbro or basalt.

To a first degree, this observation means that spreading is not systematically linked to magma extraction, even in the case of fast spreading, and that adiabatic decompression of the asthenosphere does not necessarily trigger melting. Furthermore, lateral variations in the thermal state and composition of the mantle could also influence magma generation, whereas physical processes other than asthenosphere upwelling could be involved.

Another hypothesis is that both asthenosphere partial melting and magma extraction at mid-ocean ridges are linked to plate tectonics, mainly according to the scheme of Doglioni (1990, 2003). Partial melting would occur by decoupling and/or shearing (Doglioni et al., this volume) at the interface between asthenosphere and lithosphere or in the uppermost part of the asthenosphere. In that case, mantle convection would play a minor role. Magma extraction with magma intrusion/eruption in or on the oceanic mantle lithosphere would be dependent on the rheological behavior of that lithosphere during spreading. My observations on the Chenaillet ophiolite (Montgenèvre, Franco-Italian Alps) fit with such a hypothesis. This hypothesis is analogous to the model whereby "hotspot" magma genesis and extraction are related to shallow tectonics and not to deep-seated mantle plumes, as argued in numerous papers in this volume.

CURRENT CONCEPTS OF PROCESSES THAT GIVE BIRTH TO SLOW-SPREADING OCEANS

Both the opening and slow spreading of oceans are associated with tectonic exhumation of mantle and lenticular gabbro bodies on the seafloor along the rift axis of recent (Karson et al., 1987; Dick, 1989; Cannat, 1993; Cannat and Casey, 1995; Cannat et al., 1997; Ohara et al., 2002, 2003) or fossil (Lagabrielle and Cannat, 1990; Lagabrielle and Lemoine, 1997; Rampone and Piccardo, 2000) oceans. This exhumation predates or is synchronous with basaltic eruptions, the extent of which is restricted compared to the exhumed mantle surface (Lagabrielle and Lemoine, 1997 and references therein).

The tectonic processes affecting mantle and gabbro exhumation involve simple shear along concave-downwards, low-angle detachment faults during opening (Whitmarsh et al., 2001 and references therein) and pure shear along symmetric and listric high-angle faults during spreading (Durand et al., 1996; Cannat et al., 1997; Lagabrielle et al., 1998 and references therein).

In both tectonic models, the emplacement of volcanoes in the axial zone remains enigmatic. Indeed, as far as we know (Ballard and van Andel, 1977; Ramberg and van Andel, 1977; Stakes et al., 1984; Parson et al., 1993; Smith and Cann, 1993; Smith et al., 1995a; Allerton et al., 1996; Head et al., 1996; Cannat et al., 1997; Lagabrielle et al., 1998; Searle et al., 1998a), volcanoes were never emplaced along the high-angle faults on both sides of the rift valley, but along the rift axis that overlies a fissural magmatic conduit.

Gabbros and basalts originate from distinct magmatic reservoirs resulting from partial melting of the same asthenospheric source (Bertrand et al., 1987; Rampone et al., 1995, 1996, 1998; Casey, 1997; Desmurs et al., 2002; Chalot-Prat et al., 2003). Thus, once formed, basaltic magma is either intrusive within or extrusive above the lithospheric mantle. That suggests rapidly varying rheological behavior of the suboceanic mantle as gabbros and basalts outcrop next to one another along the rift axis. It also means that fissure-fed dikes should be more or less rooted in the mantle. Thus basement exhumation and magma eruption, which occur along the axial fracture, and lateral syn-rift faults, which lead to the formation of rift shoulders, appear to be complementary in a spreading system that allows solid and melt transfer and oceans to widen.

The aim of the present study is (1) to assess better how volcano emplacement, basement exhumation, and sea floor spreading are linked; and (2) to question the link between these processes and mantle partial melting. A 1:25,000 map of an undeformed 30 km² Jurassic ophiolite was made for the Chenaillet massif (Franco-Italian Alps). The 3D geometry of this small segment of ocean floor is comparable to that described at the rift axis of a slow-spreading ocean of Atlantic type (Chalot-Prat et al., 2005). Therefore the detailed architecture of single and composite volcanic edifices (metric to kilometric scale) and the timing of emplacement of volcanoes relative to one another are constrained by both field observations and basalt geochemistry. I used the space-time relationships of volcanoes with their basement to decipher the link between mantle exhumation, volcanism, and processes of enlargement of the ocean floor. I propose a model whereby mantle melting is controlled by the relative motions of the asthenosphere and lithosphere at divergent plate boundaries.

GEOLOGICAL SETTING OF THE CHENAILLET OPHIOLITE

The Chenaillet ophiolite belongs to the Ligurian-Piemonte zone in the western Alps (Fudral, 1998) and, in particular, to an external/upper nappe that escaped subduction and only recorded

oceanic seafloor metamorphism. It is one of the rare pieces of evidence for Jurassic primary oceanic lithosphere in the Alps (Mével et al., 1978; Bertrand et al., 1981, 1982, 1987; Lagabrielle and Cannat, 1990; Caby, 1995; Lagabrielle and Lemoine, 1997; Costa and Caby, 2001; Chalot-Prat et al., 2003).

Previous authors (Mével et al., 1978; Bertrand et al., 1981, 1982, 1985, 1987; Lagabrielle et al., 1985; Lagabrielle, 1987, 1994; Lemoine et al., 1987; Lagabrielle and Cannat, 1990; Caby, 1995; Lagabrielle and Lemoine, 1997) have shown that the ophiolitic sequence consists of serpentinitized peridotites intruded by gabbro sills up to 200 m thick and truncated by an “erosional” surface. This surface is thought to be overlain by a discontinuous sequence of basalts and related hyaloclastites up to 400–1000 m thick, sometimes preceded by clastic sedimentary deposits. Bertrand et al. (1987) pointed out the mid-ocean ridge basalt (MORB) affinity of the basalts with similar compositions for dikes and their surrounding pillows. Faults of presumed Jurassic age underlying the contact between gabbro and basaltic pillows were mapped by Caby (1995). No sedimentary deposit is found above the basaltic cover. The internal structure of the ophiolitic nappe (Bertrand et al., 1982; Caby, 1995; Barféty et al., 1995, 1996) is believed to have been affected by the Alpine orogeny. The ophiolite comprises several slices thrust westwards and sometimes inverted above the slightly folded base contact of the nappe.

The recent study of Chalot-Prat et al. (2005) and this work are supported by a 1:25,000 geological map (Fig. 1A), six related cross-sections (Fig. 2), and detailed observations of the lithological units of the ophiolite. The most important result concerns the architecture of volcanoes, which permits the proposal that the original internal structure of this portion of ocean floor is preserved in the nappe. This portion represents a 30-km² surface layer of the upper part of the oceanic lithosphere, translated westwards from its original site without tilting. In the north-south direction, the arched form of the base contact of the nappe (Fig. 2A) resulted from tectonic delamination along a preexisting zone of weakness (possibly a serpentinitization front) located in the mantle protolith at a maximum of 400 m below the ocean floor. In detail, the serpentinitized mantle is partially capped by thin (≤ 50 m) and discontinuous (500 m to 5 km in length) gabbro bodies and/or a thin (50 m) and discontinuous (some m² to ~ 12 km²) volcanic cover (Fig. 2B). At the top of both serpentinites and gabbros, a locally preserved serpentinitic or gabbroic cataclasite horizon is found (10 cm to 3 m in thickness; average grain size between 0.1–1. mm, up to 50 cm), often including clasts of dolerite and basalt. Where the effects of subaerial erosion are more significant through the volcanic cover (i.e., on the flanks of the highest reliefs in the central and southeastern parts), volcanic feeder-dikes clearly crosscut and volcanoes overlie these tectonic microbreccias. This tectonic horizon, also described at the Mid-Atlantic Ridge (MAR) (Mével et al. 1991; Cannat et al. 1997), testifies to mantle and gabbro exhumation along extensional detachment faults active during eruptions (Manatschal et al. in prep.). Locally these cataclasites

are overlain by fragments, up to meters across, of fine-grained (≤ 1 mm) clastic stratified deposits reworking exclusively cataclasite fragments. These sediments, which always predate any volcanic activity, are often tilted beneath the undeformed overlying pillow edifices.

On the scale of the ophiolitic fragment, the top of the mantle basement is domed (750 m in difference of level) both in the west-east and north-south directions (Fig. 2A), and undulated on a small scale (Fig. 2B). The undulations have amplitudes of 100–400 m over areas of several 100 m². The volcanic cover and the gabbro bodies form a veneer up to 50 m thick above the mantle basement. This volcanic cover and its basement are subdivided into several blocks by major submeridian fractures, the traces of which disappear close to and on both sides of the central major volcanic edifices (Chenaillet, Grand Charvia, and Cima Saurel in Fig. 1A). As the organization of volcanoes is significantly different from one block to another, these fractures are thought to predate or even to be coeval with the eruptive activity.

In the following sections, I describe how the small- and large-scale details of this volcanic architecture increase understanding of both the geometry of volcanoes and their original structures and, except for the subaerial erosional effects, the original topography and structure of the ocean floor on the whole.

ARCHITECTURE OF INDIVIDUAL AND COMPOSITE VOLCANOES

The volcanic cover of the Chenaillet ophiolite consists of accumulations of pillows and tubes (2–10 m elongate pillows). To decipher both the geometry and building process of volcanic edifices, I concentrate first on the polarity of the pillows, their flow direction (which in return indicates the “pillow roots” and their sources), and the feeder-dikes of the pillows and their location relative to the accumulation of the pillows. The last two points are rarely discussed in papers on ophiolites. However, these observations underpin my descriptions below.

Individual Volcanoes

Tongue-like Volcano. This type of volcano (Figs. 1A, B, and 3) is well developed on the central-northern side of the Chenaillet massif (Rocher de l’Aigle massif in Fig. 1A), and on the first third of the slope around the Loubatière and Grand Charvia massifs (Fig. 1A). The tongues (Fig. 3B, parts a, b, c, and f) are 1–15 m thick, 5–70 m wide, and 10–200 m long. They are formed with interlaced lava tubes and pillows (Fig. 3B, parts d, e, f, and g) and sometimes with thin lava flows, overlain at times by accumulations of pillow breccias, 50 cm to 5 m thick (Fig. 3B, part h). The polarity of the pillows is always normal and their flow surfaces dip from a few degrees to 45° downward. They resemble cascading pillow flows (Macdonald et al., 1996; Juteau and Maury, 1999). The flow directions of the pillows are often divergent within the same tongue, the root of which can be visualized from the geometry of the tongue itself (Fig. 1A and B).

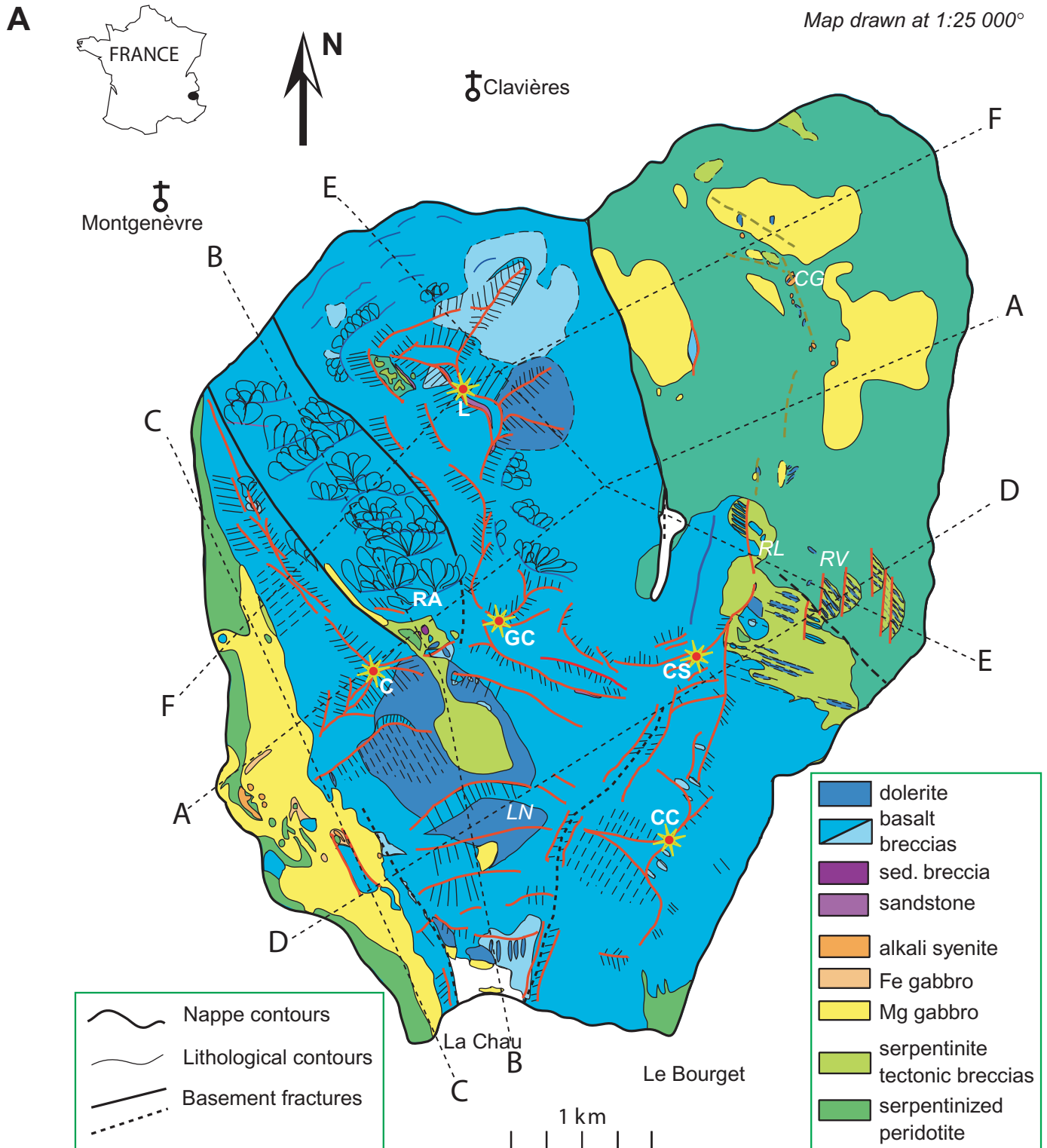


Figure 1. (A) Geological map of the Chenaillet ophiolite, Western Alps (after Chalot-Prat et al., 2005). Dotted lines A, B, C, D, E, F are cross-sections drawn on Figure 2. Abbreviations for volcanic systems are given in (B). Yellow star with red center—summits of the relief; C—Chenaillet; RA—Rocher de l’Aigle; GC—Grand Charvia; CS—Cima Saurel; CC—Crete du Chouchar; L—Loubatière; CG—Clos de la Gavie; RL—Roc la Luna; RV—Rocca Vecchia; LN—Lac Noir. (B) Architecture of the volcanic cover of the Chenaillet ophiolite and location of the geochemical sampling. Dotted lines—sampling cross sections in stair systems or sampling areas in comb systems; C/T—Chenaillet comb systems; RA/S—Rocher de l’Aigle stair system; L/S—Loubatière stair system; L/T—Loubatière comb system. Other symbols as in (A).

B

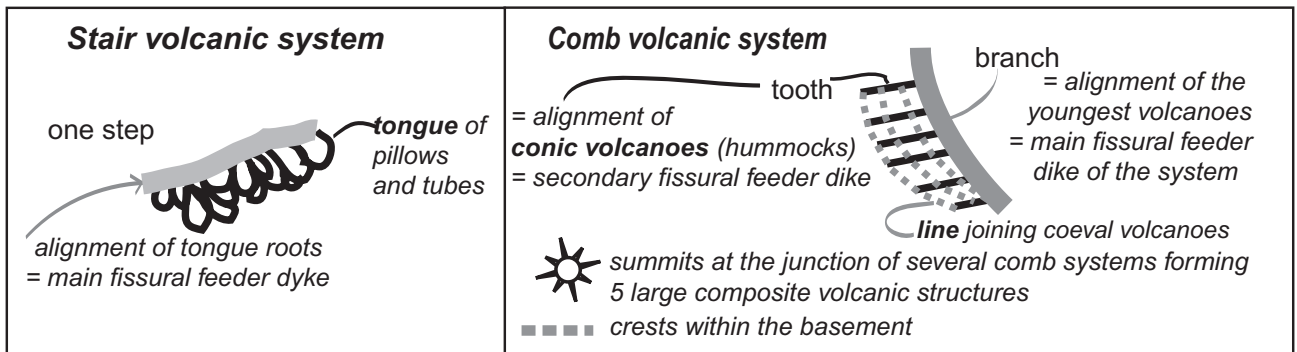
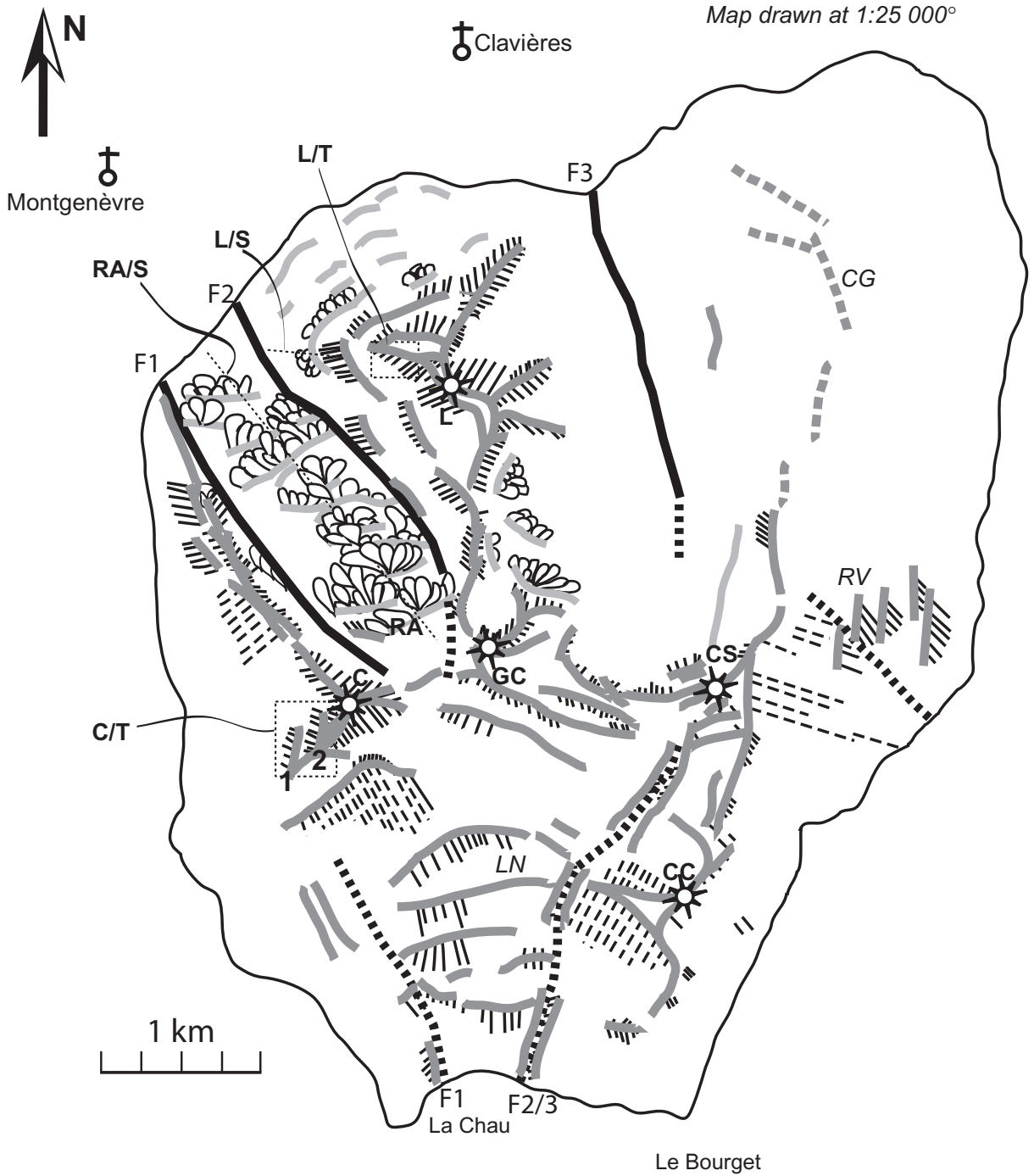
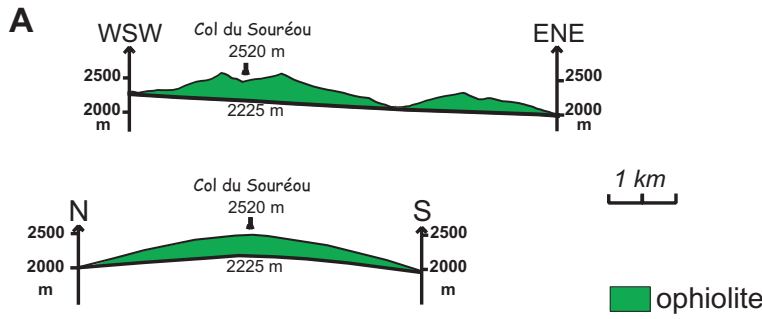
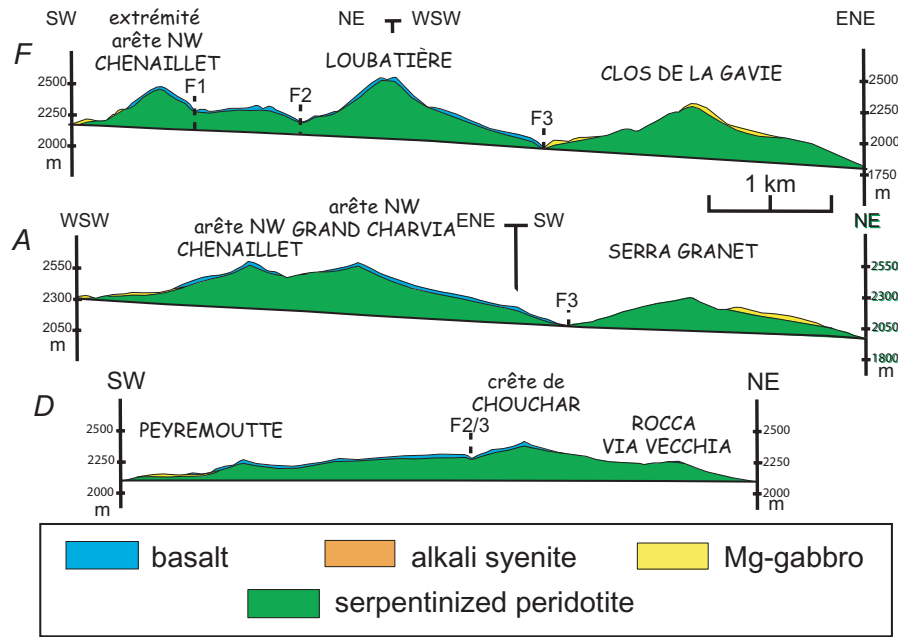


Figure 1. Continued



B W-E CROSS-SECTIONS



N-S CROSS-SECTIONS

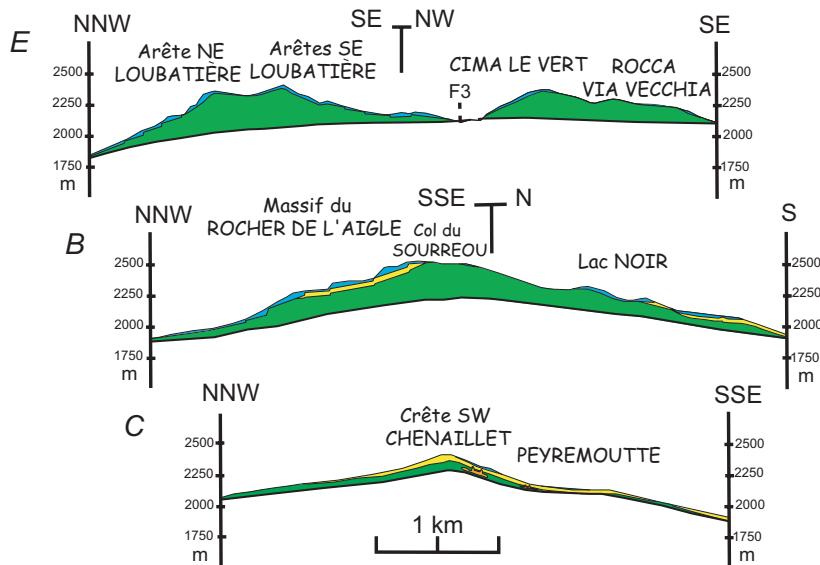


Figure 2. (A) Large-scale cross-sections in orthogonal directions of the ophiolitic nappe, showing the undulating top of the mantle basement. (B) Detailed cross-sections allowing visualization of the thickness of both the volcanic cover and the gabbro sills overlying the undulating top of the mantle basement.

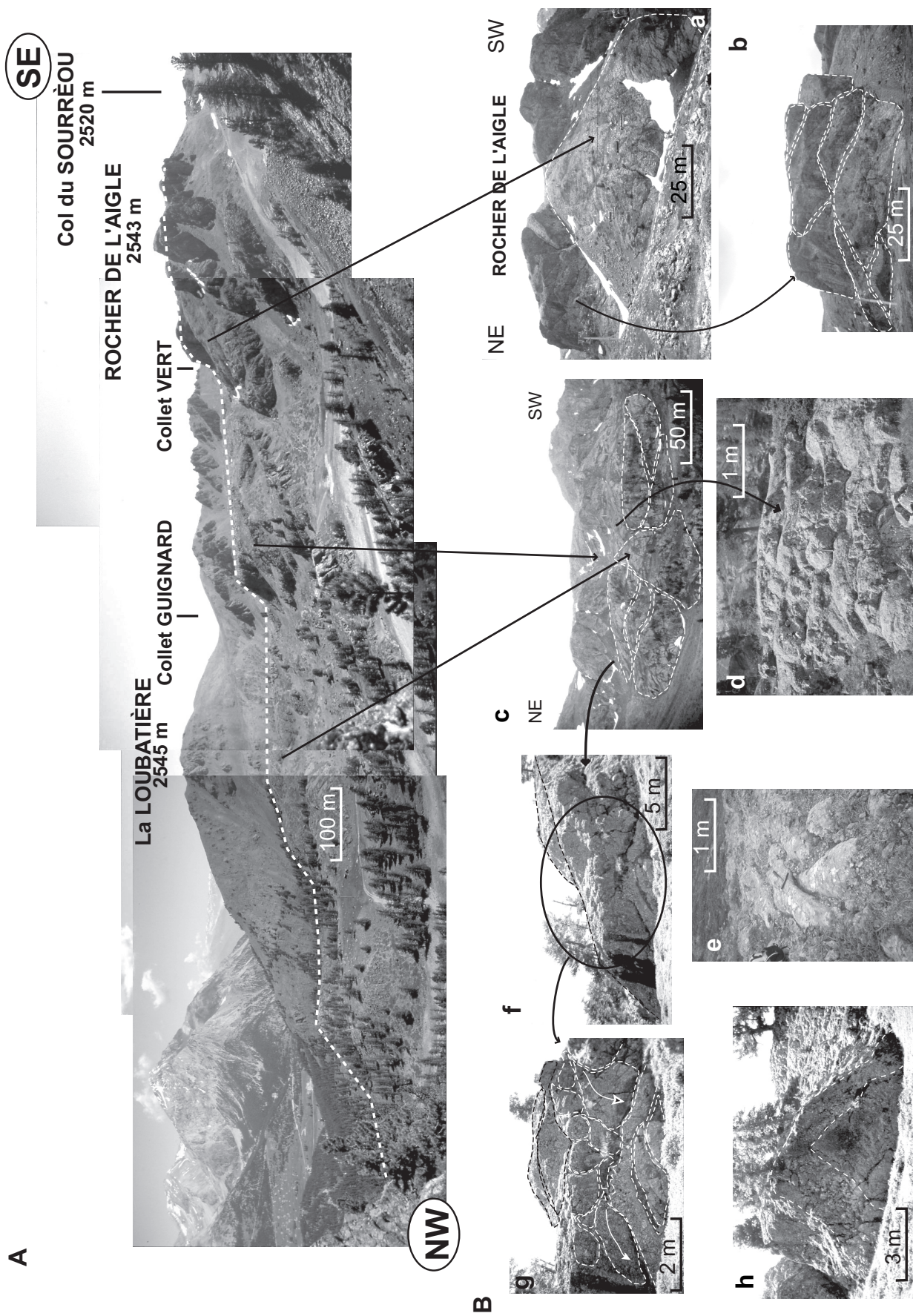


Figure 3. (A) Panorama of the stair volcanic system of the Rocher de l'Aigle viewed in profile; the white dotted line underlines the top of the successive steps of the stair; the background eastwards is formed by the volcanic hummocky ridge Loubatière–Collet Vert. (B) Detailed views of tongues of pillows and their internal structure: a and b—detailed views of the distribution of tongues within the last step; a—the tongue cascades onto the previous step; b—the view from front on different tongues fit into one another from base to top; c—view from front onto two successive steps and internal distribution of tongues; d and e—views in longitudinal section and from above of the internal distribution of tongue-forming elongate pillows; f and g—view in profile of the front of two superposed tongues coming from the right, and detailed rounded and elongate pillow organization. In g, the arrows indicate the flow direction; h—view in transverse section of a megapillow showing a massive core and a brecciated margin.

From place to place, as a result of erosional effects, the vertical or subvertical feeder-dikes of these tongues are observed cross-cutting the basement and passing through the pillows. They trend in two orthogonal directions, the dominant one being perpendicular to the flow surface (Fig. 1B; see also Fig. 6A).

Conical Volcano (Haystack or Hummock). This type of volcano (Figs. 1A, B, 4, and 5) is the most commonly observed volcano type. It outcrops on the steepest slopes and the crests of the topography. It is conic (3–30 m high and 3–15 m in section), and may be symmetric or asymmetric. It comprises an accumulation of tubes and pillows (30 cm to 1 m in section) with normal polarity and flow directions downward and divergent from and around a vertical or subvertical feeder-dike, itself covered with pillows (Fig. 4). Their external morphology is typically that of the haystacks or hummocks described at the MAR (Ballard and van Andel, 1977; Zonenshain et al., 1989; Smith and Cann, 1990, 1992, 1993; Auzende et al., 1993; Smith et al., 1995b; Head et al., 1996; Lawson et al., 1996). Frequently these volcanoes are agglomerated against one another, forming small composite edifices around several dikes (two to ten) that may be separated by pillows (Fig. 5A and C). In Figure 4, the flow directions of pillows illustrate that the conic volcanoes were built on a rather steep (45° – 80°) slope or a crest. So except for erosional effects, which reduced by up to perhaps two or three times the original volumes of the edifices, the actual slopes and crests of the relief mirror the original ones. These observations also mean that both the paleovertical and, to a lesser extent, the paleotopography are preserved. This preservation is completely unexpected in the Alps. The actual topography of the whole ophiolite is thus a structural surface except in its central (Col du Souréou) and southeastern parts (Costa via Vecchia), where erosion is much more significant and causes the basement to outcrop. In these areas, conic volcanoes are clearly emplaced on steep slopes of serpentized peridotites capped by the cataclasite horizon. The feeder-dikes are embedded into, and the pillows overlie, the cataclasite horizon. Toward their base, the feeder dikes are often slightly curved downward or even upward and appear to be uprooted. Where the volcano has been completely eroded, the root tip of the feeder-dike is slightly curved downward and forms a small bulge in the serpentized peridotites.

Composite Volcanoes

Tongue and conic volcanoes are not randomly distributed in the volcanic cover (Figs. 1A, B, 3, 5, and 6). Two types of composite volcanic edifice occur: the *stair system*, made of tongue volcanoes, and the *comb system*, made of conic volcanoes. These new terms are defined as follows.

Stair System. This composite volcanic edifice (Figs. 1A, B, 3, and 6A), 100 to ~600 m high, is made up of two to ten steps. Each step is 10–50 m thick above the basement and 20–500 m wide and comprises a pile of tongues (Fig. 3A and B, parts b and c), the roots of which underlie a common curved fissural

conduit orthogonal to the flow slope (Fig. 1B). The flow directions of the tongues, slightly divergent relative to one another on large steps, underlie the bulging profile of the system perpendicularly to the main slope. Most often, one or several tongues of an upper step cascade over tongues of the lower step (Figs. 3A, B, and 6A). Thus the higher the tongues, the younger they are relative to the others (Fig. 6A).

This architecture demonstrates that a stair system represents a single eruptive cycle. From their geometry, dimensions, and chronology of formation, these systems are analogous to the cascade systems described on slopes of abyssal hills in the axial zone of the MAR (Ballard and van Andel, 1977) and on the sides of the East Pacific ridge (Macdonald et al., 1996). Independently of both the erupted lava volumes and the spreading rate, the fissure-fed dikes can be compared to the volcanic growth faults (syn-volcanic faults serving as magma conduits) of Macdonald et al. (1996). The fissures in the stair system at the northwestern corner of the Loubatière composite volcano have a generally curved fabric.

Comb System. This composite volcanic edifice (Figs. 1A, B, 4, 5, and 6B) is the most widespread and controls the alignments of the conic volcanoes on steep slopes (45° – 80°). A comb (Figs. 1B and 6B) is defined by a branch (250 m to 1 km long) along which the youngest volcanoes are aligned. This branch is linear or curved, connected downward to several linear and parallel teeth (four to ten per comb), and always oblique (50° – 80°) relative to the branch. The teeth correspond to alignments of volcanoes (two to ten per tooth), 50–500 m in length with an elevation difference of 50–200 m. The higher the edifice, the younger it is relative to the others (Fig. 5A and C). Thus the branch of the comb often superposes the crest of the topography. Furthermore, the slope on which the volcanoes were emplaced, and often the size of volcanoes, increases upward and with time.

Viewed from above (Figs. 1B and 6B), conic volcanoes from different teeth of the same comb fall onto lines that are slightly curved, because the number of volcanoes per tooth generally increases from the boundaries toward the center of the comb. On the same line, eruptions are coeval, as shown by rhythmic variations of rock compositions from one line to another (see below). The feeder dikes of the conic volcanoes are vertical or most often dip steeply either down- or upslope. The dips in the same comb are similar. Where they dip upslope, the downslope pillows may be slightly turned upside down (e.g., some combs of the Loubatière massif).

Two volcanoes are never observed one above another, such that a comb system represents only one eruptive cycle. When the erosion effects are sufficient, as in the central, southern, and southeastern parts of the ophiolite (Fig. 1), the mantle basement capped with a cataclasite horizon outcrops from place to place on steep slopes and crests between and below more-or-less eroded conic volcanoes. The mantle basement is thus responsible for the relief shown on the six cross-sections of Figure 2B. The volcanic cover just underlines the undulations of this relief;

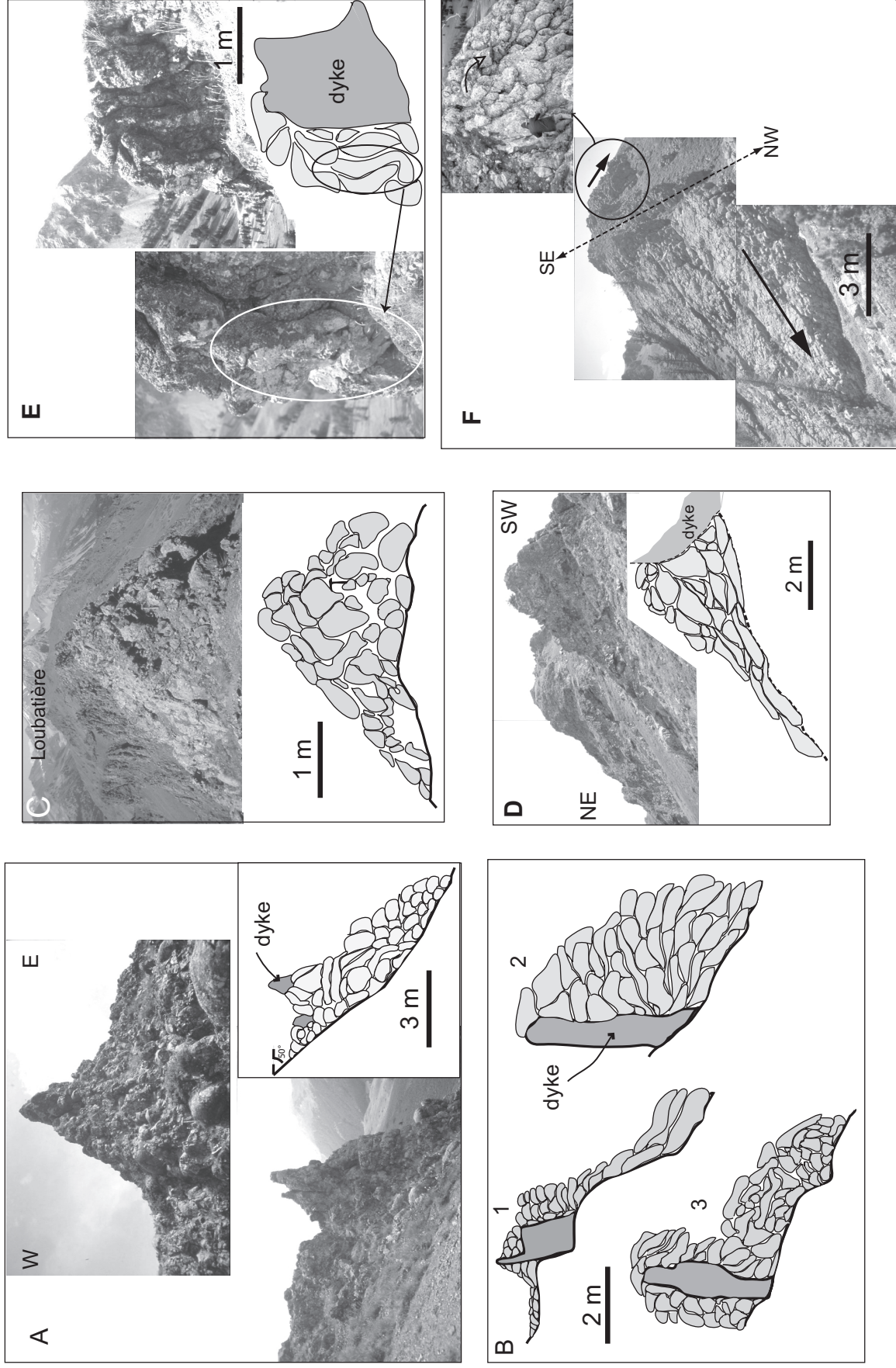


Figure 4. Drawings of pillow conic volcanoes (or hummocks) belonging to comb volcanic systems. In the same volcano, the polarity of pillows and their flow direction relative to the flow slope on the one hand, and, on the other hand, the location of the feeder-dike relative to the surrounding pillows and its subvertical dip, are complementary criteria used to decipher the architecture of the edifice, the preservation of the paleovertical, and, except for the erosion effects, the paleotopography of the volcanic cover. (A) volcano (southwest Crête du Chouchar) viewed in front and in profile; (B) different edifices in cross-section (1 and 2—Chenailliet northwest crest; 3—west Loubatière); (C) small conic volcano straddling a crest (north Collet Vert); (D) Edifice in cross-section (Chenailliet northwest crest); (E) internal part of a conic volcano with a vertical dike capped by horizontal pillows and covered on its downslope side by pillows flowing downward; (F) edifices on both sides of the same crest showing pillows with opposite flow directions (see arrows).

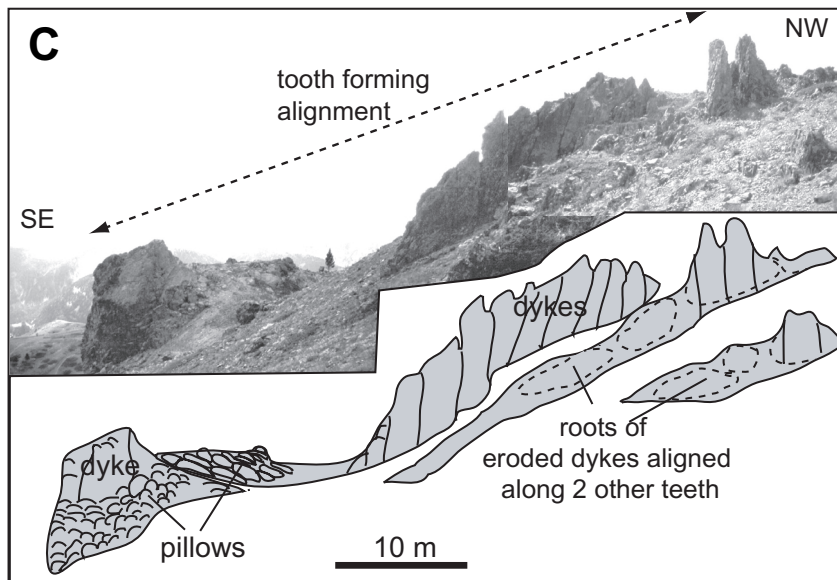
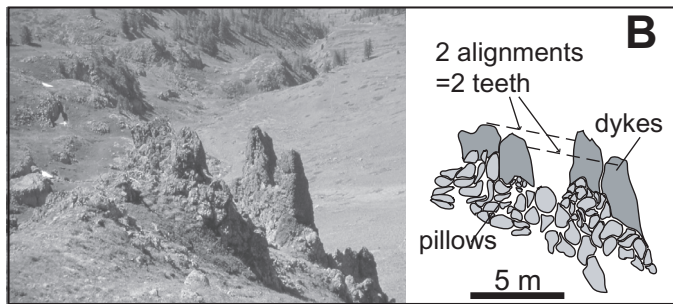
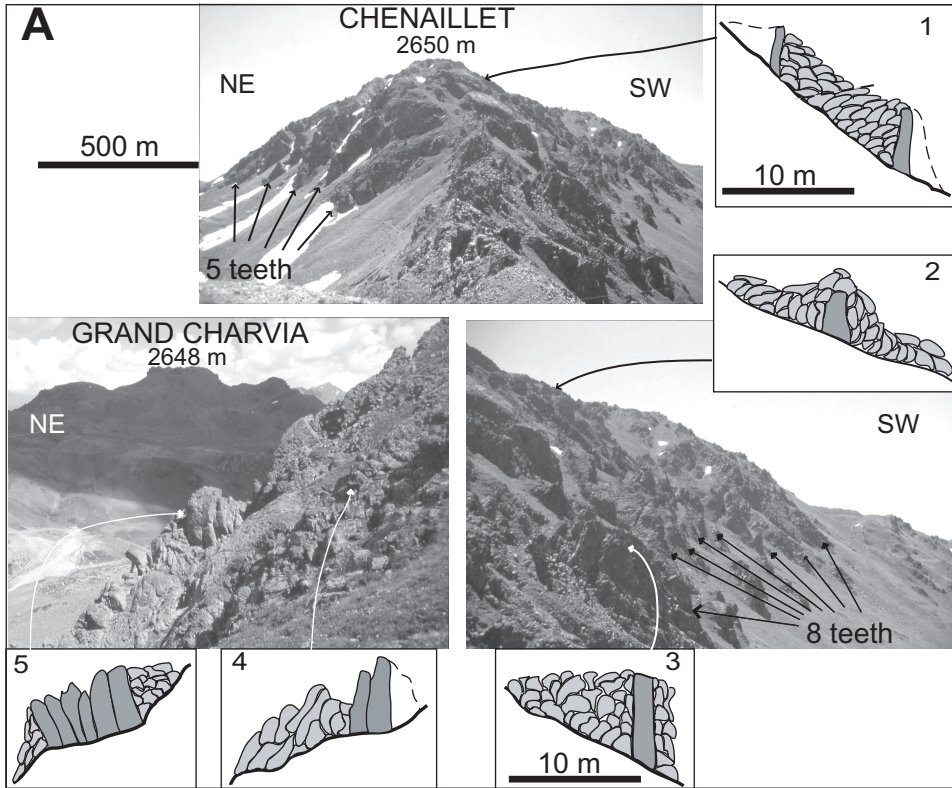


Figure 5. Comb volcanic systems and details of their internal structure. (A) Pseudo-symmetric comb systems (northwest crest of the Chenaillet composite volcano), and drawing (1–5) of internal structure of some volcanic edifices with one or several dikes in their center. In (1), the higher the edifice the younger it is relative to the other. (B) Part of a comb system viewed from the crest of a hummocky ridge (south of Collet Vert). Erosion effects cleared the pillows around the feeder-dikes. (C) Part of a comb system (north Lac Noir) with sheeted dikes along a preserved tooth.

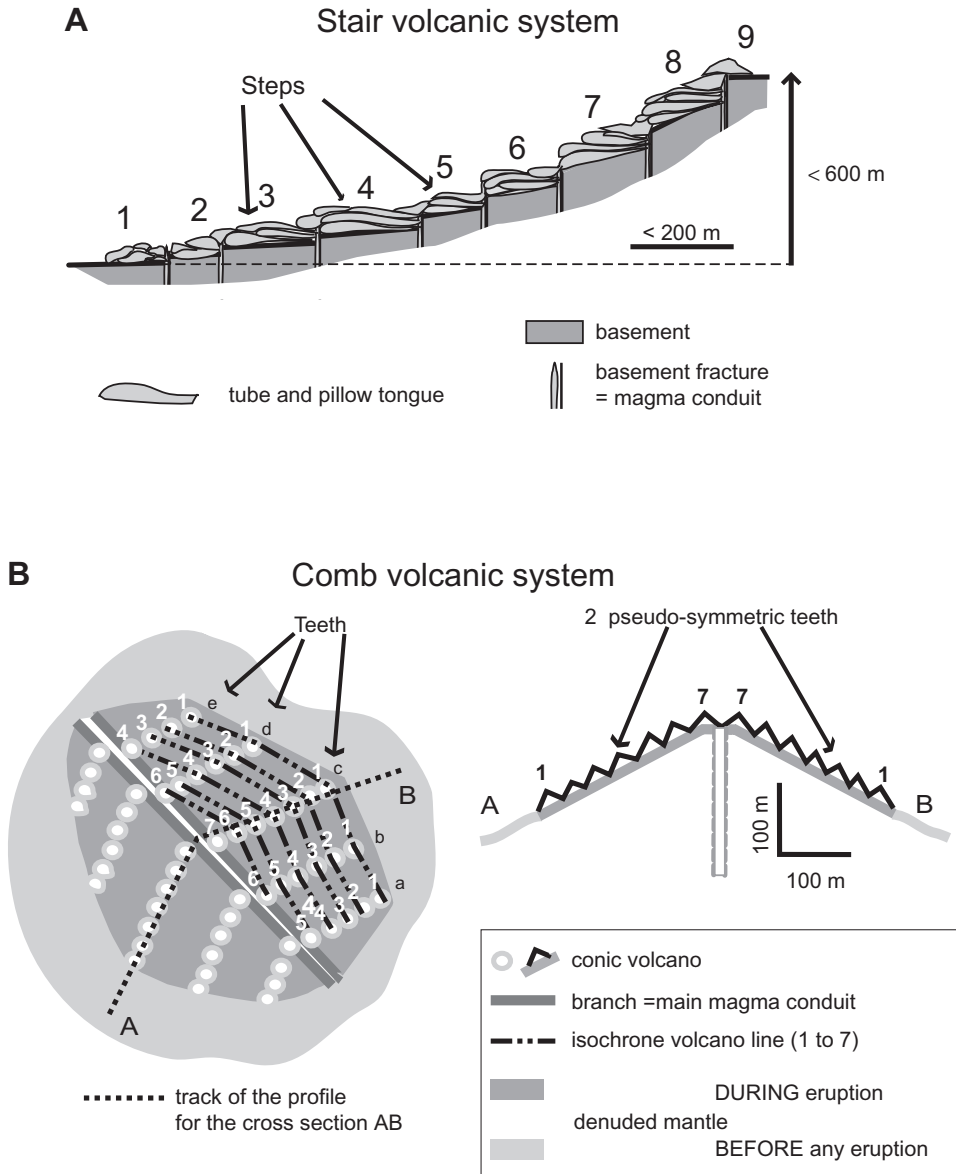


Figure 6. (A) Reconstitution of a stair volcanic system viewed in profile. Only the top of the basement crosscut by feeder-dikes is observed. (B) Reconstitution of a pseudo-symmetric comb volcanic system viewed from above and in profile.

it is thin (10–50 m) but could have been twice this thickness before erosion.

Such comb systems, the architecture of which can only be deciphered at a 1:10,000 scale, are not described elsewhere. Nevertheless Batiza and Vanko (1983) underline the importance of two directions of fractures during the building of composite volcanic structures close to the East Pacific ridge. The main direction is parallel to the long axis of the ridge, and the other is oblique by as much as 40°–50°. Small volcanoes lie at the crossings of the two fracture systems and form small chains on the flanks of composite volcanoes. Independently of the erupted lava volumes, this architecture is analogous to that of comb systems. This similarity also means that whatever the rates of oceanic spreading and crustal growth, the processes controlling the building of the volcanoes are similar.

ARCHITECTURE OF VOLCANIC SYSTEMS RELATIVE TO ONE ANOTHER AND ORIGIN OF VOLCANIC RELIEF

The stair systems are always located topographically lower than the comb systems and predate them (Fig. 1A and B). The comb systems can follow one another upward on the same slope. The higher the system, the younger it is relative to the others. They are often found on both sides of the same crest, forming pseudosymmetric structures, because their respective teeth do not trend in the same direction (Figs. 1B and 6B). On the scale of the entire volcanic zone (Fig. 1B), the youngest comb branches follow one another along crests forming several chains of segments (250 m to 1 km long and 100–700 m wide) more or less en echelon between five composite volcanoes (Chenaillet [C],

Grand Charvia [GC], Loubatière [L], Cima Saurel [CS], southern tip of Crête du Chouchar [CC]). These major volcanic centers (700–1500 m in section, 100–300 m high) are also summits above the ocean floor and resemble triple junctions. The main alignments of crests are submeridian and could have been parallel to the axial volcanic ridge. The numerous curved fissures on some flanks of two major volcanoes (L and GC) and the alignment of three major volcanoes (C, GC, and CS) in a direction orthogonal to the presumed ridge suggest transform faults. Indeed, the ridge-transform junction is characterized both by the curved fabric of fissure networks (Gudmundsson, 1995) and alignments of major volcanoes (Beutel, this volume).

On a large scale, the volcanic zone is 3–5 km wide and 100–600 m high. Thus this volcanic zone appears to have a 3D architecture and dimensions analogous on both small and large scales to those described for a volcanic abyssal hill and its hummocky ridges at the MAR and the French-American Mid-Ocean Undersea Scientific program (FAMOUS) zone (Ballard and van Andel, 1977; McDonald, 1977; Crane and Ballard, 1981; Smith and Cann, 1990, 1992, 1993; Gente et al., 1991; Allerton et al., 1995; Durand et al., 1995, 1996; Smith et al., 1995a,b; Head et al., 1996; Lawson et al., 1996).

Another striking result of the present field study concerns the undulations of the top of the mantle basement (Fig. 2A and B), whether it is overlain or not with volcanic edifices and/or exhumed gabbro sills. In addition, the undulations are most accentuated below the major composite volcanoes and the crests between them, the building of which represents the main stage of formation of the volcanic cover. This structure implies that the relief is due to uplift of the serpentinized peridotites, as also deduced by Zonenshain et al. (1989) from their observations on both volcano structures and volcanic relief at the MAR.

This hypothesis of mantle uplift has been discussed in several other papers (Ballard and van Andel, 1977; Kuo and Forsyth, 1988; Lin et al., 1990; Sempéré et al., 1990; Cannat, 1993, 1996 and references therein; Cannat et al., 1997, 1999; Searle et al., 1998b) that address the question, using seismic and gravity results, of the respective contributions of serpentinites (density lower than that of basalts) and basalts to explain the relief at the axial volcanic ridge. In the absence of any drilling, all these authors except Zonenshain et al. (1989) favored thickening of the crust without excluding the possibility of a thin crust overlying a dome of serpentinite.

RHYTHMIC CHEMICAL EVOLUTION OF BASALTS DURING THE BUILDING OF VOLCANIC SYSTEMS

To constrain the chronology of eruptions on a small scale in the comb and stair systems and to decipher the genetic relationships between basalts from successive eruptions in one system and from different systems, lavas were sampled in comb and stair systems from three key-zones (Fig. 1B): (1) two successive comb systems on the northwestern side of the Chenaillet hill; (2) one stair system on the Rocher de l'Aigle massif; and (3) one stair

and one comb system on the western side of the Loubatière hill. Before continuing to describe the observations and interpretations of the compositional variations on a small scale, I describe the sampling as a whole (Table 1).

General Features of the Lavas

As specified in Table 1, samples from the selected areas, including both pillow and dike cores, are mainly aphyric, both to the naked eye and at the microscopic scale, as already described by Bertrand et al. (1987). Nevertheless, some variations occur on the Chenaillet hill, with samples often including up to 10% phenocrysts (albitized plagioclase) and/or pseudomorphs of olivine and/or clinopyroxene (often preserved colorless salite). The same assemblage can be observed among microlites—mostly quenched microcrysts—with small additional amounts of Fe-Ti oxide, euhedral apatite, rare zircon, and titanite (Chalot-Prat et al., 2003).

In terms of major element compositions (Table 1, Fig. 7), samples are rather diverse, with Mg# (defined as $100(\text{Mg}^{2+}/[\text{Fe}_{\text{Tot}} + \text{Mg}^{2+}])$) from 50 to 66 and SiO_2 from 47% to 55%. They are in the compositional range of tholeiitic to andesitic basalts from the Atlantic and Indian oceans (Pyle et al., 1995; Le Roex et al., 1996; Kempton and Casey, 1997). As classically observed, and despite sometimes a somewhat high loss on ignition (LOI; 2.5% on average; maximum, 5%), the Mg# variations correlate positively with MgO (4–9%), CaO (6–14%), and Al_2O_3 (14–18%), and negatively with Fe_2O_3 (11–6%), TiO_2 (2.3–0.9%), SiO_2 (55–48%), and Na_2O (6.2–2%). The rather large variations of SiO_2 and Na_2O contents for the same Mg# are not correlated with LOI and thus are independent of secondary alteration. They are likely due to albitization of plagioclase with concomitant gains in Si and Na, and loss in Ca.

There is no difference in composition between aphyric and porphyritic samples, as also noted by Bertrand et al. (1987). This remark also applies to trace elements (see below). Such transition elements as Ni, Cr, and (to a lesser extent) Co are as usual positively correlated with Mg# and negatively correlated with Sn, V, and Zn.

In terms of trace element compositions (Table 1), chondrite-normalized rare earth element (REE) patterns (Fig. 8) are rather homogeneous, which means that crystal fractionation is limited. With $\text{La}_N/\text{Ce}_N \leq 1$ and $\text{La}_N/\text{Yb}_N \geq 1$ (Fig. 9), the patterns are similar to those of Indian MORB (see <http://earthref.org/GERM/reservoirs>), and closer to those of Indian enriched MORB (E-MORB) than of normal MORB (N-MORB). These patterns imply that the mantle source effects are perceptible and that basalt compositions are close to those of primitive magmas. The very low rate or even absence of crystallization of lavas supports such an interpretation. Basalts from the Loubatière (L) zone are slightly light-REE depleted compared to those from the Chenaillet (C) and Rocher de l'Aigle (RA) zones, signifying either a slight heterogeneity of the mantle source at the scale of the abyssal hill or a somewhat higher partial melting rate in the

L zone. A slight negative Eu anomaly is sometimes present in samples from the three groups. Primitive Mantle-normalized trace element patterns (Fig. 8) are rather homogeneous. All are depleted in the most incompatible elements as observed in MORB, except for a significant U enrichment in some samples. They also display somewhat pronounced Ba, Sr, and Ti negative anomalies and systematic slight Zr and Hf positive anomalies. When present, the negative Eu anomaly is not systematically correlated with Sr and Ba negative anomalies. It cannot be due to plagioclase fractionation and must be a source effect. The correlations between Zr^* ($Zr_N/[Nd_N + Sm_N]/2$) and the Nb_N/Zr_N ratio (Fig. 9) support, as for REE, an affinity for Indian MORB intermediate between N-MORB and E-MORB compositions, and mantle source effects prevail over crystal fractionation effects. In detail, Zr^* is often higher in the C and RA zones (≤ 1.8) than in the L zone (≤ 1.5). Thus as for REE fractionation, Zr fractionation relative to REE would be a tracer of a slight heterogeneity on a small scale in the mantle source.

Compositional Variations with Time in Comb and Stair Systems

For sampling, stair and comb systems were selected in three key zones (C, RA, and L; Fig. 1B) where systems were rather well preserved and accessible. Indeed, most of the comb systems outcrop on very steep slopes at the highest altitudes.

As shown previously, the higher the altitude of the volcanoes, the younger they are. Therefore in each selected stair system (RA/S and L/S), samples were collected from base to top along one cross-section and on successive steps (RA/S1 to RA/S8 on 500 m of elevation difference; L/S1 to L/S12 on 400 m of elevation difference). In each selected comb system (C/T and L/T), samples were collected along several adjacent teeth (Ta to Tn), hummock after hummock, from successive lines (as lines 1, 2, 3, etc., in Fig. 6B) progressing upward. On the northwestern side of the Chenaillet hill, the two selected comb systems follow each other upward (a lower comb with 80 m of elevation difference and two sampled teeth, C-1/Ta and C-1/Tb; an upper comb with 120 m of elevation difference and five sampled teeth, C-u/Ta to C-u/Te). On the western side of the Loubatière hill, the comb system with 200 m of elevation difference and four sampled teeth (L/Ta to L/Td) follows upward the previously mentioned stair system L/S.

The major, transition, and some trace element data (Table 1) are plotted in Figure 10 to allow the compositional variations of the erupted products to be traced as a function of time, either from one step to another upward in a stair or from one line to another upward in a comb. The results show systematic, significant, and rhythmic variations in terms of major and trace element contents recorded from one line to another in the comb systems. They are more pronounced and regular in the C than in the L combs (not shown). They indicate that each line was fed by the same magmatic injection and that a compositional change occurred from one line to another. This observation supports the

model concerning the chronology of volcano emplacement in a comb system. In the stair systems, less spectacular compositional variations occur from one step to another. The coherence of variations in the same comb or the same stair and the differences between systems in the recorded variations suggest multiple magma chambers, with each system being fed by its own magma chamber. The origin of such variations, with rather rapid variation of geochemistry with time, can be understood by examining correlations between elements.

Partial Melting, Crystal Fractionation, and Mixing Relationships among Basaltic Rocks of the Same System

To investigate the magmatic processes responsible for the rhythmic variations, I describe here only the most striking results from three systems (two combs, C-1/Ta and b and C-u/Ta to e, on the northwestern side of the Chenaillet hill; one stair, RA/S1 to S8 from the Rocher de l'Aigle). I then generalize the interpretations as far as possible to the systems of the Loubatière zone.

According to the general principles governing the relative behavior of the most incompatible trace elements and the transition elements during partial melting of lherzolites and crystal fractionation of tholeiitic basalts (Caroff, 1995 and references therein; Caroff et al., 1997), correlations between Ni or Cr or Th_N/Ta_N and Th_N or Zr^* ($Zr_N/[0.5(Nd_N + Sm_N)]$) (Fig. 11) demonstrate the existence of both partial melting and crystal fractionation relationships among basaltic rocks in each system. The higher the positive Zr anomaly, the higher is the rate of partial melting but the lower the rate of fractional crystallization.

Taking into account the chronology of eruptions on the scale of each system (Fig. 12), the results are as follows. In the C-1/Ta–C-1/Tb system, the Th_N/Ta_N versus Th_N variations trace an increase in the degree of partial melting of the mantle source. This increase indicates that magma was extracted proportionately as melting occurred (dynamic melting) and erupted. No magma chamber, *sensu stricto*, formed. In the C-u/Ta–C-u/Td system, the variations trace the repeated eruption of primary melts with one or two evolved melts erupting in between. These frequent eruptions of fresh melts suggest small, periodically replenished and tapped magma chambers. In the RA/S system, variations also trace successive injections of primary melts and their differentiates in between. As the crystal fractionation trend developed, replenishment of the chamber was probably less frequent than in the previous comb system. The distinction between partial melting and crystal fractionation processes is also shown by both the correlation between REE_N and Mg# and the evolution of Ch-normalized REE patterns (Fig. 12) with (1) a global REE enrichment with Mg# decreasing between partial melts (Mg# = 66–55) and their differentiates (Mg# = 55–50); and (2) a global REE impoverishment with Mg# increasing between successive primary melts, produced by increased partial melting of a progressively more refractory mantle source. Magma mixing between both primary and differentiated magmas is not

**TABLE 1. MAJOR AND TRACE ELEMENT DATA ON LAVAS FROM THREE SELECTED AREAS
OF THE CHENAILLET OPHIOLITE**

Field number	Chenaillet C -l/T								Chenaillet C -u/T				
	01CH157 C-l/Ta1	01CH158 C-l/Ta2	01CH159 C-l/Ta3	01CH160 C-l/Ta4	01CH38 C-l/Tb1	01CH39 C-l/Tb2	01CH40 C-l/Tb3	01CH41 C-l/Tb4	01CH42 C-u/Ta1	01CH43 C-u/Ta2	01CH44 C-u/Ta3	01CH45 C-u/Ta4	01CH46 C-u/Ta5
SiO ₂	47.21	46.15	51.87	51.02	53.95	51.73	53.12	49.69	50.99	50.98	51.56	53.19	49.82
TiO ₂	1.42	1.28	1.47	1.25	1.30	1.29	1.11	1.03	1.45	1.44	2.10	2.08	1.76
Al ₂ O ₃	17.21	15.76	14.39	15.73	14.87	16.40	14.42	16.29	15.32	15.36	14.75	15.09	15.70
Fe ₂ O ₃	10.88	10.24	8.01	7.34	7.98	8.18	9.04	7.20	8.82	8.48	10.18	8.42	10.04
MgO	7.63	8.3	4.74	5.78	7.32	5.56	6.79	6.92	7.48	6.08	5.13	4.89	6.51
MnO	0.16	0.21	0.2	0.13	0.15	0.12	0.18	0.14	0.14	0.15	0.15	0.14	0.17
CaO	6.75	10.91	13.03	8.03	6.11	8.13	7.69	11.34	7.47	8.26	8.02	7.93	8.22
Na ₂ O	4.11	2.30	4.35	6.01	5.70	5.60	5.30	4.06	5.23	5.65	5.58	6.09	4.86
K ₂ O	< L.D.	< L.D.	< L.D.	< L.D.	< L.D.	0.06	< L.D.	0.06					
P ₂ O ₅	0.23	0.21	0.26	0.21	0.23	0.22	0.19	0.19	0.26	0.24	0.3	0.34	0.27
LOI	4.21	4.47	1.52	4.33	2.22	2.54	1.99	2.97	2.67	3.20	2.08	1.67	2.45
Total	99.81	99.83	99.84	99.83	99.83	99.83	99.83	99.83	99.83	99.84	99.85	99.84	99.86
Mg#	58	62	54	61	64	57	60	66	63	59	50	53	56
SiO ₂	49.38	48.40	52.76	53.42	55.27	53.17	54.29	51.30	52.48	52.75	52.74	54.18	51.14
TiO ₂	1.49	1.34	1.50	1.31	1.33	1.33	1.13	1.06	1.49	1.49	2.15	2.12	1.81
Al ₂ O ₃	18.00	16.53	14.64	16.47	15.23	16.86	14.74	16.82	15.77	15.89	15.09	15.37	16.12
Fe ₂ O ₃	11.38	10.74	8.15	7.69	8.18	8.41	9.24	7.43	9.08	8.77	10.41	8.58	10.31
MgO	7.98	8.70	4.82	6.05	7.50	5.71	6.94	7.14	7.70	6.29	5.25	4.98	6.68
MnO	0.17	0.22	0.20	0.14	0.15	0.12	0.18	0.14	0.14	0.16	0.15	0.14	0.17
CaO	7.06	11.44	13.25	8.41	6.26	8.36	7.86	11.71	7.69	8.55	8.20	8.08	8.44
Na ₂ O	4.30	2.41	4.42	6.29	5.84	5.76	5.42	4.19	5.38	5.85	5.71	6.20	4.99
K ₂ O													
P ₂ O ₅	0.24	0.22	0.26	0.22	0.24	0.23	0.19	0.20	0.27	0.25	0.31	0.35	0.28
Total (-LOI)	100	100	100	100	100	100	100	100	100	100	100	100	100
As	< L.D.	< L.D.	< L.D.	< L.D.	< L.D.	< L.D.	< L.D.	< L.D.	< L.D.	< L.D.	< L.D.	< L.D.	< L.D.
Ba	6.95	3.15	4.22	5.96	5.87	17.38	3.68	< L.D.	5.39	5.42	4.92	4.73	14.67
Be	< L.D.	< L.D.	1.60	< L.D.	< L.D.	< L.D.	< L.D.	< L.D.	< L.D.	< L.D.	< L.D.	< L.D.	< L.D.
Bi	< L.D.	< L.D.	< L.D.	< L.D.	< L.D.	< L.D.	< L.D.	< L.D.	< L.D.	< L.D.	< L.D.	< L.D.	< L.D.
Cd	< L.D.	< L.D.	< L.D.	< L.D.	< L.D.	< L.D.	< L.D.	< L.D.	< L.D.	< L.D.	< L.D.	< L.D.	0.48
Ce	15.17	14.28	18.78	13.94	14.72	15.84	11.85	11.63	17.42	16.55	20.89	24.36	17.20
Co	42.36	34.24	19.36	32.33	31.31	34.84	24.07	33.14	33.25	33.18	33.38	30.30	37.32
Cr	332	324	175	243	303	277	300	293	273	281	123	161	188
Cs	< L.D.	< L.D.	< L.D.	< L.D.	< L.D.	< L.D.	< L.D.	< L.D.	< L.D.	< L.D.	< L.D.	< L.D.	< L.D.
Cu	17.30	37.74	22.21	60.62	26.90	61.94	15.96	14.45	96.61	72.42	82.33	56.17	76.58
Dy	4.661	4.282	5.617	4.053	4.487	4.342	3.741	3.461	5.236	5.206	6.993	7.470	6.305
Er	2.667	2.484	3.261	2.424	2.692	2.590	2.250	2.100	3.088	3.014	4.105	4.364	3.671
Eu	1.147	1.121	1.636	1.104	1.013	1.238	1.060	1.012	1.461	1.348	1.780	1.897	1.632
Ga	17.99	18.72	20.73	14.99	10.10	15.56	15.45	13.59	15.43	15.47	17.89	17.17	17.45
Gd	4.39	3.99	5.35	3.93	4.28	4.08	3.51	3.25	4.96	4.88	6.52	7.00	5.83
Ge	0.894	1.681	1.605	0.990	0.886	1.591	1.003	1.340	1.152	1.084	1.541	1.313	1.165
Hf	2.965	2.596	3.571	2.639	2.672	2.639	2.273	2.240	3.106	3.285	4.497	5.167	3.702
Ho	0.998	0.913	1.200	0.894	0.972	0.947	0.819	0.761	1.113	1.089	1.521	1.615	1.380
In	< L.D.	< L.D.	0.100	< L.D.	< L.D.	< L.D.	< L.D.	< L.D.	< L.D.	< L.D.	< L.D.	0.118	0.123
La	4.87	4.66	6.36	4.48	4.74	5.00	4.05	3.73	5.50	5.18	6.31	7.86	5.28
Lu	0.430	0.400	0.525	0.379	0.430	0.422	0.364	0.334	0.489	0.489	0.648	0.697	0.577
Mo	< L.D.	< L.D.	< L.D.	< L.D.	< L.D.	< L.D.	< L.D.	< L.D.	< L.D.	< L.D.	< L.D.	< L.D.	< L.D.
Nb	2.734	2.317	3.058	2.309	2.267	2.470	1.838	1.736	2.849	2.742	3.263	4.615	2.960
Nd	11.69	10.86	14.84	10.84	11.42	11.30	9.44	8.71	13.19	13.11	17.17	19.08	14.45
Ni	80.02	90.31	73.92	116.70	85.29	142.09	126.91	139.31	72.19	71.06	59.80	81.01	97.79
Pb	< L.D.	1.09	1.45	< L.D.	1.66	1.00	< L.D.	1.01	2.26	< L.D.	1.65	2.48	1.38
Pr	2.349	2.177	2.889	2.145	2.298	2.229	1.883	1.779	2.662	2.571	3.296	3.803	2.950
Rb	< L.D.	< L.D.	< L.D.	< L.D.	< L.D.	0.766	< L.D.	0.668					
Sb	< L.D.	< L.D.	< L.D.	< L.D.	< L.D.	< L.D.	< L.D.	< L.D.	< L.D.	< L.D.	< L.D.	< L.D.	< L.D.
Sm	3.523	3.292	4.389	3.138	3.462	3.364	2.878	2.690	4.140	3.940	5.290	5.666	4.541
Sn	1.694	2.637	2.007	1.450	2.353	1.267	1.703	1.473	2.845	1.937	2.089	3.078	2.386
Sr	186	101	343	161	165	256	164	87	145	210	158	129	325
Ta	0.227	0.186	0.259	0.195	0.188	0.209	0.160	0.159	0.245	0.238	0.285	0.374	0.245
Tb	0.716	0.650	0.866	0.624	0.693	0.665	0.575	0.537	0.788	0.797	1.072	1.157	0.966
Th	0.186	0.220	0.203	0.172	0.251	0.203	0.114	0.136	0.208	0.205	0.243	0.278	0.173
Tm	0.410	0.389	0.517	0.381	0.432	0.406	0.348	0.332	0.472	0.454	0.661	0.694	0.594
U	0.120	0.176	0.200	0.080	0.110	< L.D.	0.077	0.372	0.079	0.193	0.149	0.151	0.076
V	217	214	230	214	177	218	196	182	231	229	308	292	270
W	< L.D.	< L.D.	< L.D.	< L.D.	< L.D.	< L.D.	< L.D.	< L.D.	< L.D.	< L.D.	< L.D.	< L.D.	< L.D.
Y	29.01	26.62	34.82	25.37	25.53	26.89	25.21	21.31	32.43	33.08	45.67	47.30	42.61
Yb	2.814	2.628	3.488	2.610	2.665	2.69.01	2.360	2.186	3.235	3.197	4.181	4.511	3.743
Zn	86.75	123.07	54.00	68.34	88.46	75.55	69.13	83.85	100.70	79.90	98.21	84.57	145.06
Zr	137	125	165	126	126	132	109	97	158	144	193	242	184

Chenaillet C -u/T

<i>01CH109A</i>	<i>01CH109B</i>	<i>01CH109C</i>	<i>01CH107A</i>	<i>01CH107B</i>	<i>01CH107C</i>	<i>01CH108A</i>	<i>01CH108B</i>	<i>01CH108C</i>	<i>01CH110A</i>
C-u/Tb1	C-u/Tb2	C-u/Tb3	C-u/Tc1	C-u/Tc2	C-u/Tc3	C-u/Td1	C-u/Td2	C-u/Td3	C-u/Te1
50.30	51.51	51.02	50.11	50.38	52.98	50.76	51.26	48.87	53.99
1.44	2.10	1.14	1.46	2.14	1.79	1.41	2.14	1.14	1.39
15.52	14.49	16.31	15.70	15.57	14.41	15.47	14.72	16.52	15.06
8.55	10.29	7.30	8.74	10.79	9.04	8.76	10.50	7.75	7.96
5.78	5.53	6.72	6.34	5.75	5.69	6.06	5.51	6.62	5.32
0.15	0.16	0.15	0.13	0.18	0.17	0.18	0.15	0.13	0.18
10.91	7.87	9.40	10.00	7.08	7.72	9.58	7.48	11.60	7.98
4.57	5.75	4.90	4.66	5.49	5.97	4.96	5.60	3.91	6.07
< L.D.									
0.25	0.29	0.22	0.23	0.28	0.31	0.27	0.29	0.21	0.25
2.37	2.49	2.69	2.48	2.70	1.76	2.38	2.15	3.08	1.64
99.84	100.48	99.85	99.85	100.36	99.84	99.83	99.80	99.83	99.84
57	52	65	59	51	55	58	51	63	57
51.61	52.57	52.51	51.46	51.59	54.02	52.09	52.49	50.51	54.98
1.48	2.14	1.17	1.50	2.19	1.83	1.45	2.19	1.18	1.42
15.92	14.79	16.79	16.12	15.94	14.69	15.87	15.07	17.07	15.34
8.77	10.50	7.51	8.98	11.05	9.22	8.99	10.75	8.01	8.11
5.93	5.64	6.92	6.51	5.89	5.80	6.22	5.64	6.84	5.42
0.15	0.16	0.15	0.13	0.18	0.17	0.18	0.15	0.13	0.18
11.19	8.03	9.67	10.27	7.25	7.87	9.83	7.66	11.99	8.13
4.69	5.87	5.04	4.79	5.62	6.09	5.09	5.73	4.04	6.18
0.26	0.30	0.23	0.24	0.29	0.32	0.28	0.30	0.22	0.25
100	100	100	100	100	100	100	100	100	100
< L.D.									
4.47	3.03	9.29	3.14	3.83	< L.D.	< L.D.	< L.D.	< L.D.	5.44
< L.D.									
< L.D.									
< L.D.									
17.98	21.51	12.91	16.07	20.50	21.68	16.88	21.65	12.83	16.84
31.37	32.23	33.38	31.10	30.71	32.96	33.70	34.53	31.24	31.24
276	126	271	254	114	197	265	123	261	256
< L.D.									
81.53	54.79	40.57	56.15	59.23	61.85	118.92	56.64	29.31	134.13
5.275	7.342	3.811	5.033	6.998	6.630	4.928	7.481	3.816	5.029
3.108	4.256	2.231	2.930	4.355	4.063	2.910	4.364	2.230	2.906
1.526	1.768	1.075	1.405	1.814	1.673	1.392	1.774	1.219	1.471
16.62	18.47	12.90	16.17	19.85	14.73	15.29	17.31	15.22	14.53
4.99	6.87	3.48	4.71	6.70	6.19	4.72	6.95	3.54	4.72
1.364	1.381	0.883	1.374	0.970	1.022	1.191	1.384	1.182	1.188
3.051	4.101	2.313	3.029	4.321	4.096	3.073	4.321	2.318	3.203
1.118	1.543	0.817	1.082	1.541	1.446	1.046	1.554	0.824	1.070
< L.D.	0.115	< L.D.	< L.D.	< L.D.	0.108	< L.D.	0.114	< L.D.	< L.D.
5.73	6.40	4.16	5.15	6.27	6.76	5.40	6.52	4.11	5.45
0.489	0.612	0.350	0.464	0.677	0.630	0.459	0.679	0.339	0.461
0.68	0.46	< L.D.							
2.740	3.319	2.052	2.798	3.200	3.452	2.686	3.363	2.059	2.654
13.22	16.98	9.43	12.74	17.33	17.33	12.58	17.51	9.64	12.81
67.59	60.18	125.18	63.07	54.43	100.23	67.39	60.59	125.14	65.52
1.13	1.56	1.60	1.50	1.85	1.32	1.75	1.04	< L.D.	2.03
2.757	3.448	1.961	2.564	3.297	3.447	2.558	3.428	1.982	2.613
< L.D.									
0.14	< L.D.								
3.842	5.358	2.807	3.851	5.401	5.236	3.669	5.340	3.018	3.814
1.514	2.113	1.057	1.680	2.367	2.214	2.203	1.920	1.362	2.341
178	90	286	107	106	70	83	124	94	165
0.229	0.272	0.175	0.230	0.289	0.318	0.218	0.283	0.171	0.218
0.806	1.126	0.592	0.782	1.076	1.074	0.744	1.126	0.585	0.767
0.192	0.230	0.121	0.185	0.219	0.247	0.169	0.207	0.125	0.199
0.500	0.659	0.351	0.464	0.655	0.623	0.484	0.709	0.342	0.457
0.244	0.156	0.097	0.118	0.129	0.144	0.090	0.113	0.073	0.125
228	302	200	220	281	240	223	301	199	224
< L.D.									
30.82	44.04	23.18	31.25	44.66	40.40	30.57	44.59	23.75	30.66
3.114	4.218	2.189	2.989	4.386	4.037	3.021	4.437	2.302	2.942
68.28	93.37	61.14	77.67	114.01	106.24	115.03	88.74	55.39	75.07
145	193	115	156	188	207	144	198	114	143

(continued)

TABLE 1. Continued

Field number	Rocher de l'Aigle RA/S							
	01CH156 RA/S1	01CH155 RA/S2	01CH154 RA/S3	01CH153B RA/S4	01CH152 RA/S5	01CH151 RA/S6	01CH150 RA/S7	01CH49 RA/S8
SiO ₂	50.63	52.68	48.99	51.51	51.65	51.84	47.76	52.44
TiO ₂	1.56	1.64	1.27	1.73	1.68	1.66	1.5	1.43
Al ₂ O ₃	15.55	15.55	15.33	15.45	15.96	15.71	16.12	15.34
Fe ₂ O ₃	9.25	8.83	8.09	9.64	8.9	8.9	8.5	8.74
MgO	6.31	5.44	5.98	5.12	5.67	5.36	4.88	5.72
MnO	0.14	0.15	0.14	0.15	0.15	0.15	0.16	0.14
CaO	8.44	7.72	10.61	7.9	7.11	7.31	12.21	8.04
Na ₂ O	5.11	5.89	4.79	5.34	5.9	5.96	4.11	5.63
K ₂ O	0.06	< L.D.	< L.D.	0.26	< L.D.	< L.D.	< L.D.	< L.D.
P ₂ O ₅	0.24	0.25	0.2	0.26	0.26	0.25	0.25	0.15
LOI	2.54	2.22	4.41	2.46	2.55	2.69	4.34	2.19
Total	99.83	100.37	99.81	99.82	99.83	99.83	99.83	99.82
Mg#	57	55	59	51	56	54	53	56
SiO ₂	52.04	53.67	51.35	52.91	53.09	53.37	50.02	53.71
TiO ₂	1.6	1.67	1.33	1.78	1.73	1.71	1.57	1.46
Al ₂ O ₃	15.98	15.84	16.07	15.87	16.41	16.17	16.88	15.71
Fe ₂ O ₃	9.51	9	8.48	9.9	9.15	9.16	8.9	8.95
MgO	6.49	5.54	6.27	5.26	5.83	5.52	5.11	5.86
MnO	0.14	0.15	0.15	0.15	0.15	0.15	0.17	0.14
CaO	8.68	7.87	11.12	8.11	7.31	7.53	12.79	8.24
Na ₂ O	5.25	6	5.02	5.48	6.06	6.14	4.3	5.77
K ₂ O	0.06	0.27	0.1	0.96	0.1	0.07	0.14	1
P ₂ O ₅	0.25	0.25	0.21	0.27	0.27	0.26	0.26	0.15
Total (-LOI)	100	100	100	100	100	100	100	100
As	< L.D.	< L.D.	< L.D.	< L.D.	< L.D.	< L.D.	< L.D.	< L.D.
Ba	7.95	8.62	9.41	9.18	10.05	10.29	8.47	18.92
Be	< L.D.	< L.D.	< L.D.	< L.D.	< L.D.	< L.D.	< L.D.	< L.D.
Bi	< L.D.	< L.D.	< L.D.	< L.D.	< L.D.	< L.D.	< L.D.	< L.D.
Cd	< L.D.	< L.D.	< L.D.	0.32	< L.D.	< L.D.	< L.D.	< L.D.
Ce	17.36	16.81	11.68	15.99	19.02	18.7	17.09	10.9
Co	34.75	35.45	34.62	36.07	35.77	32.91	35.54	34.57
Cr	218	223	253	159	184	173	195	245
Cs	< L.D.	< L.D.	< L.D.	< L.D.	< L.D.	< L.D.	< L.D.	< L.D.
Cu	75.28	63.08	79.66	65.24	62.06	55.47	58.36	55.68
Dy	5.579	5.632	4.339	5.671	5.669	5.591	5.21	5.191
Er	3.312	3.393	2.513	3.361	3.493	3.367	3.045	3.2
Eu	1.549	1.462	1.149	1.5	1.467	1.549	1.504	1.164
Ga	16.44	16.92	14.71	16.89	17.05	16.93	18.85	14.18
Gd	5.2	5.37	3.93	5.36	5.33	5.3	4.77	4.399
Ge	1.438	1.229	1.542	1.333	1.402	1.374	2.23	1.446
Hf	3.337	3.551	2.625	3.682	3.932	3.491	3.034	2.661
Ho	1.219	1.241	0.926	1.223	1.181	1.202	1.079	1.094
In	0.106	< L.D.	< L.D.	< L.D.	< L.D.	< L.D.	< L.D.	0.085
La	5.42	5.25	3.56	4.95	6.06	6.04	5.79	3.327
Lu	0.521	0.516	0.409	0.517	0.554	0.51	0.457	0.517
Mo	< L.D.	0.48	< L.D.	< L.D.	< L.D.	< L.D.	< L.D.	< L.D.
Nb	2.711	2.858	2.009	2.831	2.99	2.776	2.601	1.761
Nd	13.61	13.76	9.5	13.54	14.04	14.28	12.85	10.34
Ni	103.17	102.39	127.06	74.44	90.25	75.65	105.83	125
Pb	1.35	1.17	2.05	1.38	0.92	1.7	1.6	< L.D.
Pr	2.744	2.746	1.861	2.563	2.91	2.906	2.723	1.916
Rb	0.89	< L.D.	< L.D.	2.96	< L.D.	< L.D.	< L.D.	< L.D.
Sb	< L.D.	< L.D.	< L.D.	< L.D.	< L.D.	< L.D.	< L.D.	< L.D.
Sm	4.157	4.264	3.058	4.314	4.063	4.173	3.763	3.455
Sn	2.791	1.995	2.785	2.026	1.742	1.774	1.544	1.132
Sr	152	224	186	154	166	105	47	202
Ta	0.224	0.239	0.182	0.247	0.264	0.259	0.229	0.149
Tb	0.848	0.874	0.662	0.881	0.934	0.859	0.785	0.777
Th	0.175	0.189	0.14	0.211	0.231	0.212	0.185	0.12
Tm	0.52	0.539	0.403	0.519	0.543	0.542	0.474	0.482
U	0.076	0.128	0.146	0.223	0.381	0.099	0.144	0.075
V	243	251	222	259	265	244	234	217
W	< L.D.	< L.D.	< L.D.	< L.D.	< L.D.	< L.D.	< L.D.	< L.D.
Y	34.15	36.48	27.62	38.03	34.23	32.37	29.81	31.54
Yb	3.312	3.35	2.713	3.529	3.452	3.319	3.108	3.257
Zn	78.5	82.77	72.14	84.63	81.81	81.44	73.96	65.02
Zr	153	169	117	168	170	153	146	112

Loubatière L/S

02CH19 L/S1	02CH20 L/S2	02CH21 L/S3	02CH22 L/S4	02CH24 L/S5	02CH23 L/S6	02CH25 L/S7	02CH26 L/S8	02CH27 L/S9	02CH28 L/S10	02CH30 L/S11	02CH31 L/S12
50.57	51.08	52.05	54.15	56.59	49.41	50.81	52.36	53.43	49.09	51.33	52.46
1.58	1.6	1.54	1.46	1.42	1.27	1.35	1.61	1.56	1.59	1.88	1.44
15.64	15	16.06	14.55	14.6	16.7	16.13	15.51	15.37	16.28	15.12	15.81
9.83	9.31	8.39	8.19	6.82	7.65	7.01	8.39	8.7	9.27	8.92	9.06
6.72	6.02	5.04	4.21	3.85	5.92	4.59	5.83	4.92	6.27	5.77	4.82
0.15	0.14	0.13	0.11	0.11	0.13	0.14	0.13	0.12	0.15	0.14	0.19
8.09	9.31	8.2	9.75	8.1	10.4	13.43	8.44	7.2	9.88	8.99	8.12
4.96	4.83	5.9	5.41	4.64	4.53	3.39	5.15	6.29	4.28	4.86	5.08
< L.D.	< L.D.	< L.D.	0.1	0.93	0.1	< L.D.	< L.D.	0.07	0.14	< L.D.	0.98
0.17	0.18	0.17	0.18	0.19	0.16	0.16	0.18	0.19	0.18	0.23	0.17
2.58	2.33	2.31	1.69	2.06	3.1	3.24	2.19	1.97	2.69	2.53	2.23
100.29	99.8	99.79	99.8	99.31	99.37	100.25	99.79	99.82	99.82	99.77	100.36
58	56	54	50	53	61	56	58	53	57	56	51
51.76	52.41	53.4	55.19	58.19	51.32	52.38	53.65	54.6	50.54	52.79	53.46
1.62	1.64	1.58	1.49	1.46	1.32	1.39	1.65	1.59	1.64	1.93	1.47
16.01	15.39	16.48	14.83	15.01	17.35	16.63	15.89	15.71	16.76	15.55	16.11
10.06	9.55	8.61	8.35	7.01	7.95	7.23	8.6	8.89	9.54	9.17	9.23
6.88	6.18	5.17	4.29	3.96	6.15	4.73	5.97	5.03	6.46	5.93	4.91
0.15	0.14	0.13	0.11	0.11	0.14	0.14	0.13	0.12	0.15	0.14	0.19
8.28	9.55	8.41	9.94	8.33	10.8	13.84	8.65	7.36	10.17	9.25	8.27
5.08	4.96	6.05	5.51	4.77	4.71	3.49	5.28	6.43	4.41	5	5.18
0.17	0.18	0.17	0.18	0.2	0.17	0.16	0.18	0.19	0.19	0.24	0.17
100	100	100	100	100	100	100	100	100	100	100	100
1.719	< L.D.	< L.D.	0.926	< L.D.	< L.D.	< L.D.	< L.D.	0.865	1.937	< L.D.	< L.D.
7.94	4.67	6.61	6.63	11.92	6.52	6.4	5.53	9.51	9.79	10.01	15.28
< L.D.	< L.D.	< L.D.									
< L.D.	< L.D.	< L.D.									
< L.D.	< L.D.	< L.D.									
15.04	14.87	12.96	12.05	12.31	11.61	13.86	13.02	12.88	14.75	17.44	12.48
37.13	33.17	32.91	30.72	29.18	31.7	26.86	31.89	34.69	32.94	30.69	33.16
206	202	231	181	184	263	222	201	214	180	145	228
< L.D.	< L.D.	< L.D.	< L.D.	0.227	< L.D.	0.22	0.521				
58.34	45.26	53.1	44.03	59.72	55.27	43.75	47.9	54.12	58.11	55.95	54.42
5.774	5.725	5.592	5.052	5.233	4.345	4.845	5.759	5.608	5.359	6.64	5.287
3.4	3.482	3.395	3.074	3.148	2.637	2.858	3.424	3.446	3.183	3.982	3.289
1.405	1.556	1.398	1.313	1.348	1.234	1.462	1.425	1.439	1.468	1.698	1.291
16.28	16.14	14.82	16.22	14.6	15.05	15.92	13.54	13.97	17.91	15.11	14.09
5.169	5.172	4.955	4.497	4.527	3.909	4.355	5.074	5.003	4.892	6.065	4.693
1.348	1.85	1.964	2.545	2.023	1.702	2.178	1.698	1.939	2.114	1.317	1.889
3.183	3.117	3.021	2.745	2.833	2.441	2.71	3.199	3.115	3.126	3.909	2.904
1.197	1.186	1.187	1.063	1.099	0.922	1.01	1.199	1.205	1.128	1.384	1.132
0.082	0.083	0.087	0.083	0.08	0.082	0.092	0.092	0.087	0.086	0.093	0.074
4.856	4.812	4.111	3.822	3.761	3.774	4.607	3.873	3.944	4.743	5.62	3.883
0.523	0.531	0.524	0.462	0.486	0.395	0.43	0.541	0.532	0.508	0.63	0.53
< L.D.	< L.D.	0.418	< L.D.	< L.D.	0.538	0.463	< L.D.	< L.D.	< L.D.	< L.D.	< L.D.
2.31	2.229	2.14	1.934	2.229	1.973	2.431	2.474	2.37	2.13	1.894	2.672
12.92	13.19	11.73	11.19	11.11	9.93	11.4	12.02	11.97	12.55	15.11	11.37
91.06	104.4	109.8	92.77	93.48	106.2	105.6	97.04	107.9	77.73	64.92	111.5
1.5316	< L.D.	1.9843	< L.D.	< L.D.							
2.51	2.514	2.261	2.128	2.106	1.938	2.264	2.298	2.275	2.488	2.957	2.134
< L.D.	0.645	0.792	0.825	11.87	< L.D.	< L.D.	< L.D.	< L.D.	1.356	< L.D.	13.88
< L.D.	< L.D.	< L.D.									
4.166	4.258	3.895	3.664	3.617	3.084	3.569	4.048	4.05	3.985	4.847	3.615
1.374	1.381	1.342	1.22	1.223	1.249	1.378	1.442	1.263	1.258	1.577	1.375
219	90	124	76	87	141	110	80	139	184	175	118
0.194	0.205	0.191	0.17	0.178	0.2	0.207	0.211	0.18	0.185	0.252	0.173
0.896	0.889	0.863	0.797	0.808	0.682	0.755	0.89	0.871	0.847	1.026	0.819
0.159	0.156	0.158	0.14	0.153	0.159	0.183	0.169	0.147	0.147	0.198	0.147
0.514	0.535	0.518	0.459	0.472	0.384	0.414	0.519	0.511	0.495	0.587	0.489
0.089	0.06	0.067	0.06	0.057	0.079	0.127	0.073	0.065	0.063	0.084	0.064
239	237	227	220	216	210	221	242	230	233	266	224
< L.D.	< L.D.	< L.D.									
34.04	35.02	33.69	30.77	31.35	25.81	28.81	34.67	33.73	31.63	39.72	32.1
3.46	3.53	3.401	3.08	3.146	2.63	2.706	3.396	3.349	3.201	3.908	3.273
79.11	76.29	68.22	64.63	61.68	61.02	46.57	68.76	74.25	75.84	82.43	70.66
136	135	127	113	120	110	120	136	131	129	161	125

(continued)

TABLE 1. *Continued*

Loubatière L/T								
Field number	02CH33 L/Ta1	02CH34 L/Ta2	02CH37 L/Ta3	02CH38 L/Ta4	02CH32 L/Tb1	02CH35 L/Tb2	02CH36 L/Tb3	02CH39 L/Tb4
SiO ₂	51.55	48.13	49.71	49.23	48.81	48.67	48.63	48.73
TiO ₂	1.46	1.54	1.55	1.88	1.30	1.49	1.44	1.61
Al ₂ O ₃	15.31	15.71	16.10	15.09	15.88	15.76	15.75	16.02
Fe ₂ O ₃	8.90	8.33	8.56	10.01	8.10	8.55	8.20	8.84
MgO	6.15	5.63	5.92	5.21	6.01	5.48	5.5	5.3
MnO	0.28	0.13	0.14	0.15	0.16	0.13	0.15	0.13
CaO	6.96	12.82	10.09	11.20	10.55	12.27	11.40	12.48
Na ₂ O	5.42	3.28	4.17	3.26	4.03	3.37	4.22	2.06
K ₂ O	< L.D.	< L.D.	< L.D.	< L.D.	0.05	< L.D.	0.05	< L.D.
P ₂ O ₅	0.18	0.18	0.19	0.21	0.15	0.17	0.17	0.18
LOI	2.68	4.07	3.35	3.59	4.49	3.88	4.73	5.05
Total	98.89	99.82	99.78	99.83	99.53	99.77	100.24	100.40
Mg#	58	57	58	51	59	56	57	54
SiO ₂	53.58	50.27	51.55	51.15	51.36	50.76	50.92	51.11
TiO ₂	1.52	1.61	1.61	1.95	1.37	1.55	1.51	1.69
Al ₂ O ₃	15.91	16.41	16.70	15.68	16.71	16.44	16.49	16.80
Fe ₂ O ₃	9.25	8.70	8.88	10.40	8.52	8.92	8.59	9.27
MgO	6.39	5.88	6.14	5.41	6.32	5.71	5.76	5.56
MnO	0.29	0.14	0.15	0.16	0.17	0.14	0.16	0.14
CaO	7.23	13.39	10.46	11.64	11.10	12.80	11.94	13.09
Na ₂ O	5.63	3.43	4.32	3.39	4.24	3.51	4.42	2.16
K ₂ O	0.05	0.05	1.52	0.08	0.51	0.05	0.20	0.25
P ₂ O ₅	0.19	0.19	0.20	0.22	0.16	0.18	0.18	0.19
Total (-LOI)	100	100	100	100	100	100	100	100
As	< L.D.	0.702	0.727	0.712				
Ba	16.77	9.16	10.88	6.27	11.73	8.92	8.24	5.50
Be	< L.D.							
Bi	< L.D.							
Cd	< L.D.							
Ce	12.18	15.47	16.2	19.07	11.31	14.87	13.27	16.81
Co	33.94	29.97	30.61	36.96	33.02	30.66	30.42	29.36
Cr	232	178	181	123	278	173	182	188
Cs	< L.D.	< L.D.	< L.D.	< L.D.	0.209	< L.D.	< L.D.	< L.D.
Cu	51.29	53.88	54.51	53.47	68.09	52.46	55.10	47.49
Dy	5.391	5.235	5.270	7.164	4.642	4.995	4.947	6.013
Er	3.290	3.062	3.094	4.186	2.869	2.967	2.907	3.555
Eu	1.315	1.429	1.434	1.771	1.218	1.362	1.300	1.611
Ga	14.41	17.75	16.35	17.96	15.87	18.30	16.67	21.01
Gd	4.669	4.585	4.698	6.399	4.114	4.612	4.402	5.41
Ge	1.311	1.903	1.491	1.470	1.396	1.728	1.442	1.490
Hf	2.882	3.116	3.166	4.197	2.654	2.993	2.965	3.558
Ho	1.137	1.076	1.081	1.446	0.994	1.040	1.023	1.222
In	0.079	0.086	0.078	0.099	0.071	0.091	0.095	0.090
La	3.872	5.319	5.417	6.052	3.717	5.025	4.303	5.474
Lu	0.519	0.476	0.472	0.653	0.451	0.461	0.451	0.562
Mo	< L.D.	0.409	< L.D.	0.725	< L.D.	0.451	0.453	0.736
Nb	1.987	2.881	2.875	2.823	2.092	2.633	2.732	2.561
Nd	11.22	12.43	12.79	16.53	10.23	12.08	11.05	14.19
Ni	115.7	86.33	89.52	65.42	132.5	86.89	81.65	85.75
Pb	< L.D.	< L.D.	1.784	1.5174	< L.D.	< L.D.	< L.D.	< L.D.
Pr	2.123	2.472	2.566	3.197	1.924	2.397	2.170	2.758
Rb	0.765	< L.D.	< L.D.	< L.D.	< L.D.	0.602	1.040	< L.D.
Sb	< L.D.							
Sm	3.657	3.789	3.820	5.130	3.251	3.649	3.521	4.401
Sn	1.203	1.343	1.416	1.626	1.796	1.474	1.324	1.474
Sr	245	99	132	65	117	96	142	66
Ta	0.174	0.250	0.252	0.244	0.183	0.232	0.236	0.216
Tb	0.839	0.799	0.831	1.137	0.704	0.782	0.760	0.947
Th	0.149	0.207	0.208	0.203	0.150	0.206	0.189	0.192
Tm	0.496	0.463	0.476	0.645	0.421	0.460	0.449	0.541
U	0.077	0.088	0.112	0.090	0.163	0.132	0.164	0.146
V	222	224	236	258	215	223	226	229
W	< L.D.							
Y	32.32	30.03	31.01	41.63	27.69	29.5	28.79	35.57
Yb	3.315	3.060	3.180	4.330	2.807	3.045	2.980	3.709
Zn	74.28	69.91	68.02	89.1	66.89	65.45	66.54	70.31
Zr	122	140	143	177	112	132	132	152

Notes: Arrows indicate base and top of each tooth or each stair. Major element data by inductive coupled plasma-absorption element spectrometry and trace element data by inductive coupled plasma-mass spectrometry on whole rocks (Service d'Analyse des Roches et des Minéraux; Centre de Recherches Pétrographiques et Géochimiques-Centre National de la Recherche Scientifique, Nancy, France). Abbreviations: < L.D., below lower detection limit; LOI, loss on ignition.

Loubatière L/T

02CH50 L/Tc1	02CH51 L/Tc2	02CH52 L/Tc3	02CH53 L/Tc4	02CH40 L/Tc5	02CH56 L/Td1	02CH55 L/Td2	02CH54 L/Td4	02CH41 L/Td5
49.65	50.33	50.99	50.86	49.23	49.26	50.38	48.67	49.95
1.77	1.56	1.49	1.72	1.83	1.73	1.90	1.87	1.93
15.63	15.89	16.22	15.09	15.52	15.59	14.84	15.20	15.20
9.71	8.13	8.79	9.15	10.25	10.02	10.36	10.53	10.70
6.42	5.84	6.71	5.92	6.03	6.18	5.73	6.01	6.01
0.16	0.14	0.16	0.14	0.15	0.18	0.18	0.18	0.17
8.04	9.87	6.67	9.62	9.09	8.97	8.72	9.05	7.53
3.66	4.43	5.12	3.98	4.65	4.37	5.25	4.49	5.21
1.47	0.08	0.49	0.05	0.19	0.24	0.1	0.18	< L.D.
0.21	0.19	0.19	0.21	0.22	0.22	0.25	0.21	0.23
3.21	3.26	2.90	3.06	2.66	2.94	2.57	2.87	2.53
99.93	99.72	99.73	99.80	99.82	99.70	100.28	99.26	99.46
57	59	60	56	54	55	52	53	53
51.33	52.18	52.66	52.57	50.67	50.91	51.56	50.49	51.53
1.83	1.62	1.54	1.78	1.88	1.79	1.94	1.94	1.99
16.16	16.47	16.75	15.60	15.97	16.11	15.19	15.77	15.68
10.04	8.43	9.08	9.46	10.55	10.36	10.60	10.92	11.04
6.64	6.05	6.93	6.12	6.21	6.39	5.86	6.24	6.20
0.17	0.15	0.17	0.14	0.15	0.19	0.18	0.19	0.18
8.31	10.23	6.89	9.94	9.36	9.27	8.92	9.39	7.77
3.78	4.59	5.29	4.11	4.79	4.52	5.37	4.66	5.38
0.10	0.19							
0.22	0.20	0.20	0.22	0.23	0.23	0.26	0.22	0.24
100	100	100	100	100	100	100	100	100
1.034	< L.D.							
30.12	11.05	10.36	9.96	10.92	11.06	11.02	8.11	7.11
< L.D.								
< L.D.								
< L.D.								
17.44	15.98	14.47	16.27	17.6	16.73	19.61	17.95	18.68
33.04	30.22	32.26	32.46	32.86	33.53	32.76	33.55	34.18
142	183	181	173	158	160	122	119	105
0.611	< L.D.	< L.D.	< L.D.	0.206	< L.D.	< L.D.	< L.D.	< L.D.
58.53	58.37	54.47	52.87	53.10	57.44	54.21	59.39	56.09
6.551	5.220	5.022	6.443	6.935	6.666	7.080	7.048	7.204
3.852	3.153	2.991	3.831	4.060	3.946	4.245	4.164	4.282
1.694	1.438	1.358	1.576	1.717	1.683	1.784	1.761	1.874
17.87	16.98	14.86	15.47	18.12	17.43	17.43	17.47	17.63
5.865	4.835	4.551	5.771	6.235	5.979	6.278	6.354	6.577
1.340	1.640	1.074	1.443	1.772	1.475	1.747	1.460	1.404
3.766	3.178	3.008	3.938	4.160	4.010	4.232	4.061	4.145
1.363	1.087	1.047	1.338	1.435	1.367	1.477	1.468	1.470
0.093	0.091	0.093	0.090	0.099	0.092	0.100	0.093	0.120
5.501	5.185	4.618	4.926	5.579	5.072	6.189	5.604	5.998
0.607	0.504	0.479	0.615	0.650	0.619	0.677	0.670	0.674
0.444	< L.D.	< L.D.	0.492	0.429	< L.D.	< L.D.	< L.D.	< L.D.
2.618	2.842	2.754	2.736	2.741	2.648	2.751	2.626	2.836
15.06	12.83	12.01	14.34	15.60	14.82	16.75	15.97	16.38
76.49	83.81	79.71	79.26	75.22	81.3	61.09	64.23	60.07
< L.D.	< L.D.	< L.D.	< L.D.	1.9019	< L.D.	< L.D.	< L.D.	< L.D.
2.914	2.569	2.364	2.787	2.981	2.833	3.252	3.079	3.118
17.780	1.054	7.034	< L.D.	2.516	2.929	< L.D.	2.088	< L.D.
< L.D.								
4.789	3.979	3.681	4.642	4.952	4.724	5.214	5.127	5.211
1.520	1.491	1.229	1.514	1.720	1.673	1.993	1.738	1.757
125	162	87	125	177	119	156	122	141
0.233	0.251	0.236	0.229	0.243	0.240	0.258	0.236	0.243
1.026	0.836	0.797	0.998	1.075	1.046	1.107	1.105	1.120
0.225	0.213	0.195	0.200	0.198	0.207	0.205	0.195	0.206
0.592	0.478	0.452	0.587	0.630	0.596	0.642	0.627	0.656
0.091	0.085	0.080	0.082	0.088	0.102	0.102	0.081	0.093
255	233	226	229	256	241	245	261	273
< L.D.								
39.42	31.64	30.2	37.51	41.71	39.29	42.05	41.7	42.89
3.940	3.257	3.070	3.939	4.288	3.980	4.350	4.293	4.410
86.16	65.5	69.52	73.23	84.94	89.26	94.22	90.62	90.67
160	141	134	166	172	166	178	167	174

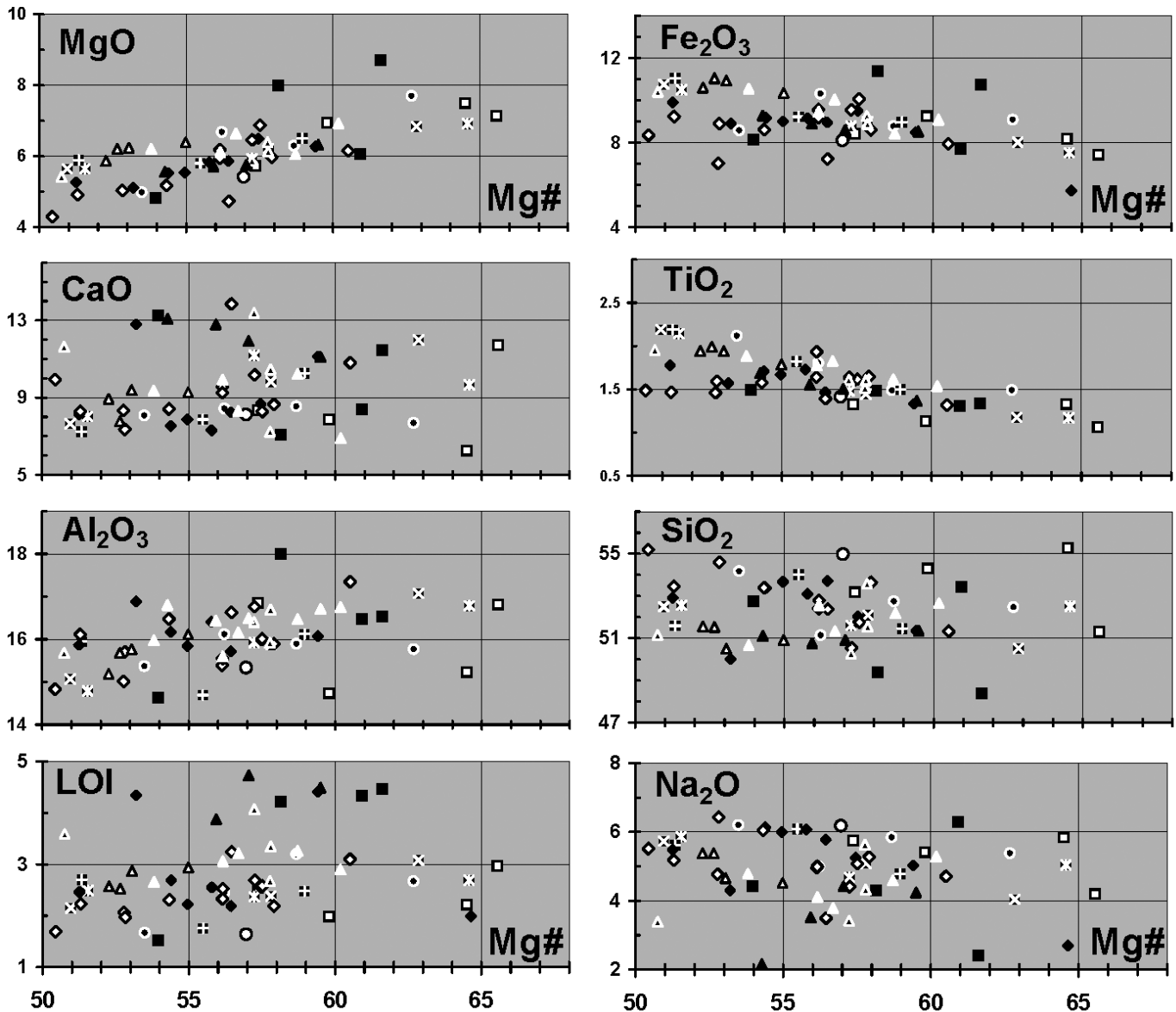


Figure 7. Variations of major element oxide contents versus Mg# (as differentiation index) in basaltic and andesitic basaltic lavas. Variations in water lost on ignition (LOI) do not show any obvious correlation with gain or loss in Na₂O. Chenaillet lower comb systems (C-l/T): black square—tooth a (al-a4); white square—tooth b (bl-b4); Chenaillet upper comb systems (C-u/T): black circle—tooth a (al-a5); star in square—tooth b (bl-b3); plus in square—tooth c (cl-c3); cross in square—tooth d (dl-d3); white circle—tooth e (el); Rocher de l'Aigle stair system (RA/S): black diamond—(S1-S8); Loubatière stair system (L/S): white diamond (S1-S12); Loubatière comb system (L/T): black triangle with white contour—tooth a (Tal-Ta4); black triangle—tooth b (Tbl-Tb4); white triangle—tooth c (Tcl-Tc4); white triangle with black contour—tooth d (Tdl-Td4).

excluded and can account for some irregularities; for example, negative Eu anomalies in fresh melts (C-l/Tb1 and RA/S8) not associated with a negative Sr anomaly in Primitive Mantle--normalized trace element patterns.

In comparison, variations of major, transition, and trace elements in basalts from the L/S and L/T systems are similar to, but somewhat less accentuated than, in basalts from the C and RA zones. Existing correlations (Fig. 11) also provide evidence

for partial melting and crystal fractionation relationships, the former likely prevailing over the latter. This last observation is supported by the general aphyric texture of lavas and the invariably quenched nature of microcrysts of olivine and plagioclase pseudomorphs. These observations imply that the liquids remained above their liquidus temperatures up to the surface and rose very quickly. It also indicates that, as for the C1 system, magma was extracted proportionately as melting occurred. In

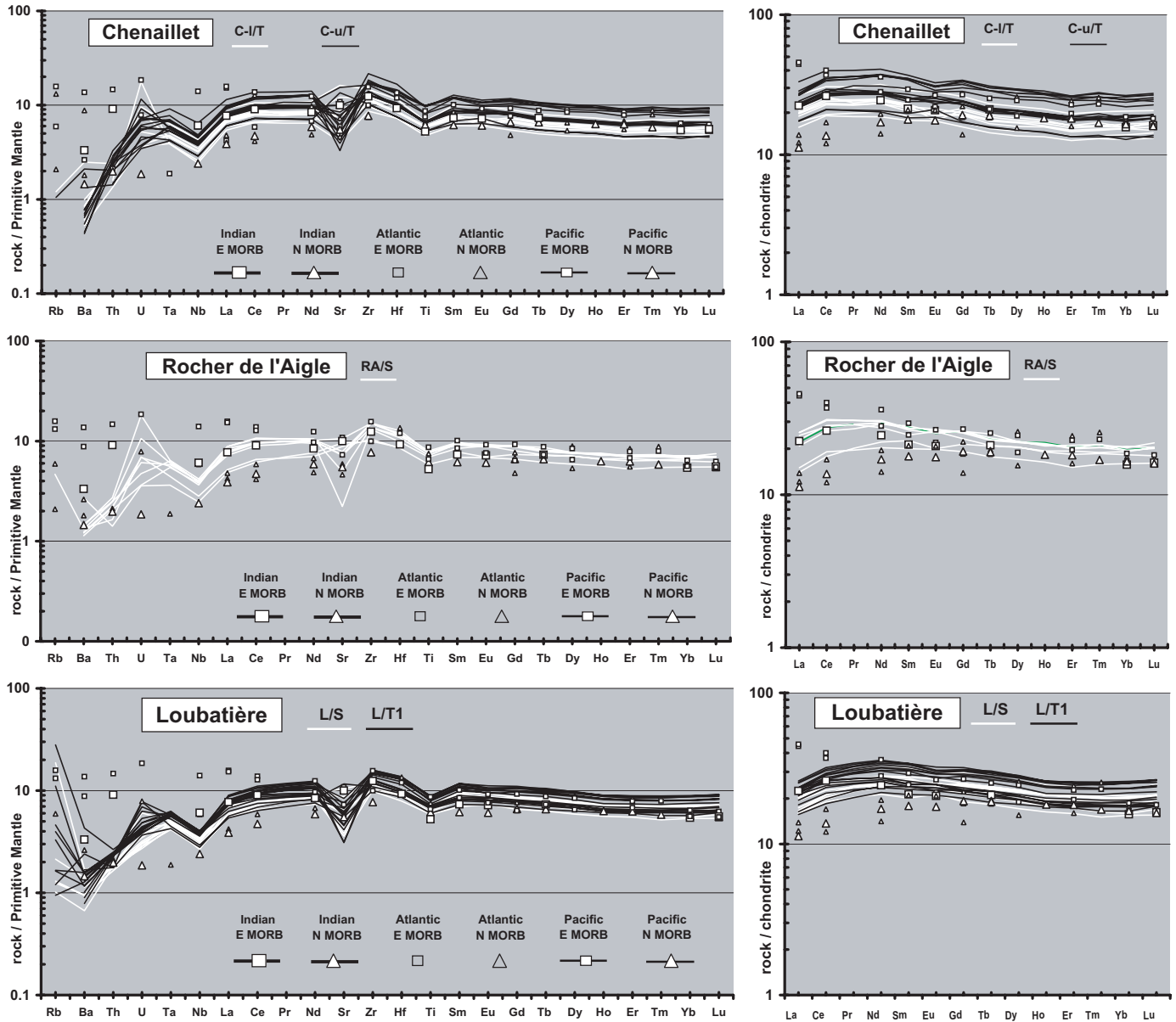


Figure 8. Primitive Mantle-normalized trace-element and Chondrite-normalized rare earth element patterns of basaltic lavas from the three sampling areas, compared to those of reference compositions of normal (N) and enriched (E) Mid-Oceanic Ridge Basalts (MORB) from Indian, Atlantic, and Pacific oceans (<http://earthref.org/GERM/reservoirs>). Note the strong similarities of sampled lavas with Indian MORB. Same legend for samples as in Figure 7.

addition, trace element patterns from the L zone are somewhat different from those from the C and RA zones, suggesting a slightly more depleted mantle source for the L basalts.

However, the composition of primary basaltic melts indicated by the relationships among the most incompatible trace elements and constrained by the covariations in Ni, Cr, Mg#, and RRE contents have lower Mg# and higher SiO₂ contents than do primitive liquid compositions (Mg# ≥ 70–75; SiO₂ ≤

48%). These are determined either from melt inclusions (Caroff, 1995) or from experimental investigations assuming a homogeneous mantle source (Green, 2000, 2001 and references therein; Presnall et al., 2002 and references therein).

In summary, the geochemical study demonstrates that each volcanic system, the geometry and timing of emplacement of which were determined from field observations, is also characterized by a homogeneous chemical dataset with coherent variations

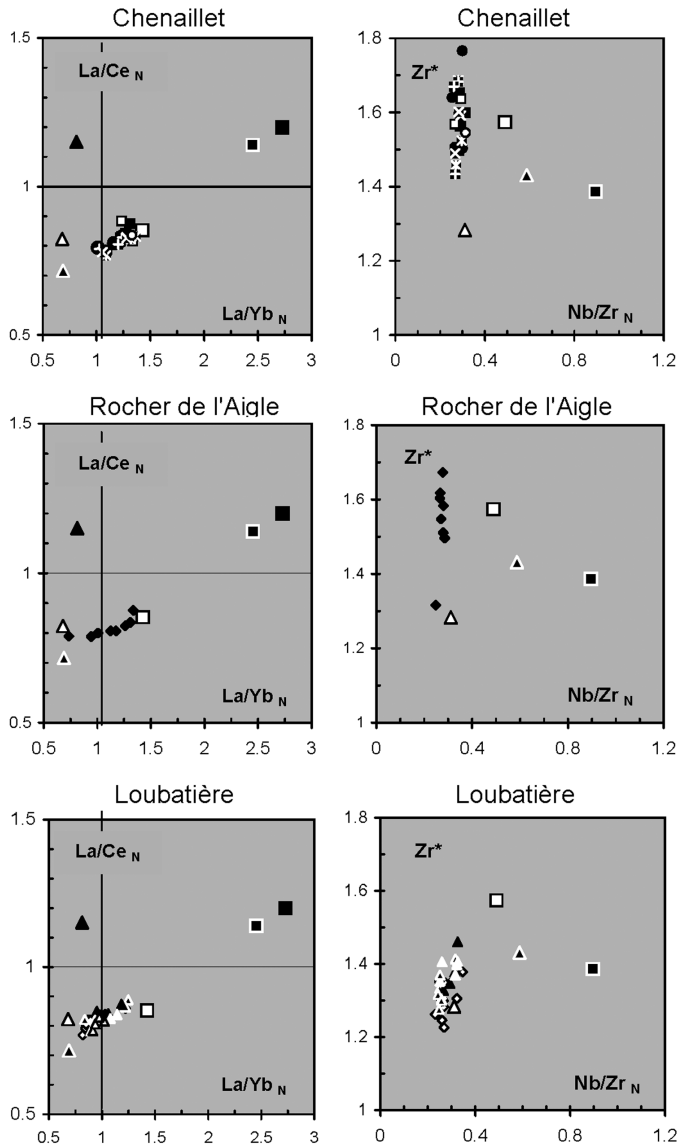


Figure 9. La/Ce_N versus La/Yb_N and Zr^* versus Nb/Zr_N diagrams showing similar features between sampled lavas and Indian MORB reference samples. Same legend for samples as in Figure 7, and for MORB references as in Figure 8.

between them. Furthermore, and most importantly, it appears that in each comb system, volcanoes were fed in line along different teeth. That the timing of eruptions is related to an increase in partial melting of the mantle source also supports the chronology of emplacement of volcanoes from base to top in the comb system.

Complementary results enable further understanding of the link between partial melting and magma extraction up to the surface. On the whole, the formation of volcanoes reflects the eruption of both partial melts from a depleted asthenospheric mantle and their differentiates by fractional crystallization. The rapid alternation of both types of product implies that the

magma conduit of each system was rooted in a small, frequently fed reservoir. The shape of these reservoirs was likely elongate (250 m to 1 km in length, as the comb branch) and narrow (several to tens of meters wide). The numerous systems that could be built synchronously in a composite volcano (see Fig. 1B) and from one composite volcano to another are an effect of the multiplicity of independent reservoirs, a hypothesis already considered by Stakes et al. (1984) and Pezard et al. (1992) for recent spreading ridges. Furthermore, that magma was often extracted proportionately as melting occurred in the same comb even suggests that the main magmatic conduit for each system was rooted close to or even in the mantle source. This configuration fits with the superheated nature of magmas deduced from the aphyric texture of lavas, as also highlighted by Stakes et al. (1984). Therefore all the main magma conduits corresponded to a network of deep fractures at the axial volcanic zone, fractures that opened up to the surface during mantle melting. Thus the strong “coupling of the eruptive process to the mechanical extension in the ridge environment” (Stakes et al., 1984, p. 6996) was both ephemeral and cyclic, accounting for the small volume of magma ($\ll 1 \text{ km}^3$) erupted during the building of each comb or stair and the successive building of several combs on each flank of hummocky ridges. The reservoirs were also ephemeral, as demonstrated by the variations of lava composition from one system to another on the same flank.

BUILDING PROCESSES OF VOLCANOES AND LINKS WITH LITHOSPHERIC SPREADING

The field observations of the stair system (Figs. 1A, B, 3, and 6A) suggest that as shown in Figure 13, it was built by uplift and step-by-step fracturing of an already denuded basement, with magma injection along fissures that formed successively from the base to the top of the stair. In this way, the same flow direction is preserved throughout the eruptive cycle leading to the building of the stair. In addition, as the dip of the flow slope increased with time, tongues from upper/younger steps can sometimes cascade onto lower/older ones.

I summarize the field observations on the comb system (Figs. 1A, B, 4, 5, and 6B) before detailing the proposed building model (Fig. 14). In space (Fig. 6B), coeval conic volcanoes, mostly separated from one another, are distributed on slopes along parallel lines that are slightly convex relative to the linear branch of the comb, which often overlies the crest of the ridge. Thanks to the effects of erosion locally, the volcanoes appear uprooted above the cataclastic horizon capping the mantle or gabbro basement. In time (Fig. 6B), from the lowest/earliest to the highest/youngest lines, volcanoes were emplaced on steeper and steeper slopes. They are separated from one another and aligned on teeth that are parallel but oblique to the branch of the comb, which superposes the youngest volcanoes of the system.

In Figure 14, these in-line volcanoes are believed to have formed on a basement in the process of uplift, at the intersections between a steeply dipping, deep, major fracture and a set of shal-

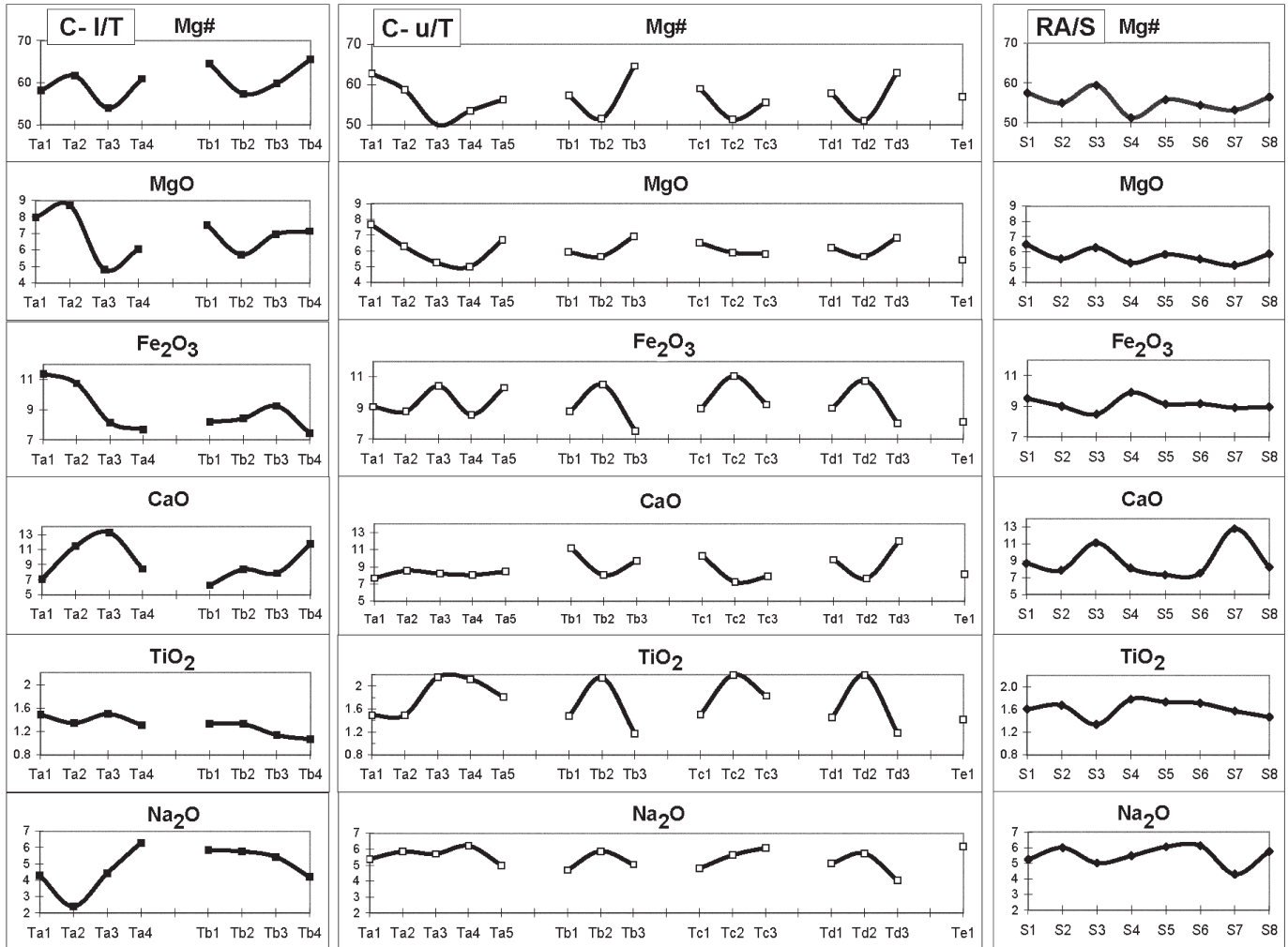


Figure 10. Rhythmic variations of Mg# and major element oxides from one line to another within the two comb systems of Chenaillet (C-I/T and C-u/T) and the stair system of Rocher de l'Aigle (RA/S).

low, parallel, secondary fractures (or tears) oblique to the major fracture. The major fracture was rooted in a magma chamber and served as a conduit to transport the magma up to the surface. The set of subsurface tears, always oblique to the major fracture, was probably linked to lithospheric stretching, as demonstrated experimentally by Tron and Brun (1991).

Once formed, volcanoes were dragged away and downward from the ridge in the spreading direction to make room for a new line of volcanoes (Fig. 14). This transport was due to the coeval exhumation of new basement (mantle or gabbro), the top of which was underlain by a detachment fault. Meanwhile the volcanoes were uprooted. Thus the building of a comb system was synchronous with an enlargement by some hundreds of meters of the basement surface.

At depth, this detachment fault overlay the wall of the deep major fracture, which served as a feeder-dike for the magma. The magma reservoir remained located beneath the shallower part of

the ridge in formation, as concluded also by Smith and Cann (1999) for the Atlantic axial volcanic ridge. In return, the existence of hummocks and seamounts on the flanks of the Atlantic Volcanic ridge can be explained with the model proposed here.

In addition, most comb structures are pseudosymmetric, with the same dip of feeder-dikes on both sides of the crests of narrow ridges, whereas the teeth of each comb have different directions and lengths (Fig. 1B). This arrangement provides evidence that the exhumation process occurred in roughly opposite directions, synchronously but at different rates.

Along the narrow crests of the relief, the major fractures are en echelon and often curved, as also observed at the MAR and Reykjanes ridge (Dauteuil and Brun, 1993; Appelgate and Shor, 1994). These observations fit well with a model of low-obliquity rifting in which the stretching direction forms an angle equal to or greater than 45° with the plate boundaries (Tron and Brun, 1991).

These results have several implications. A majority of the

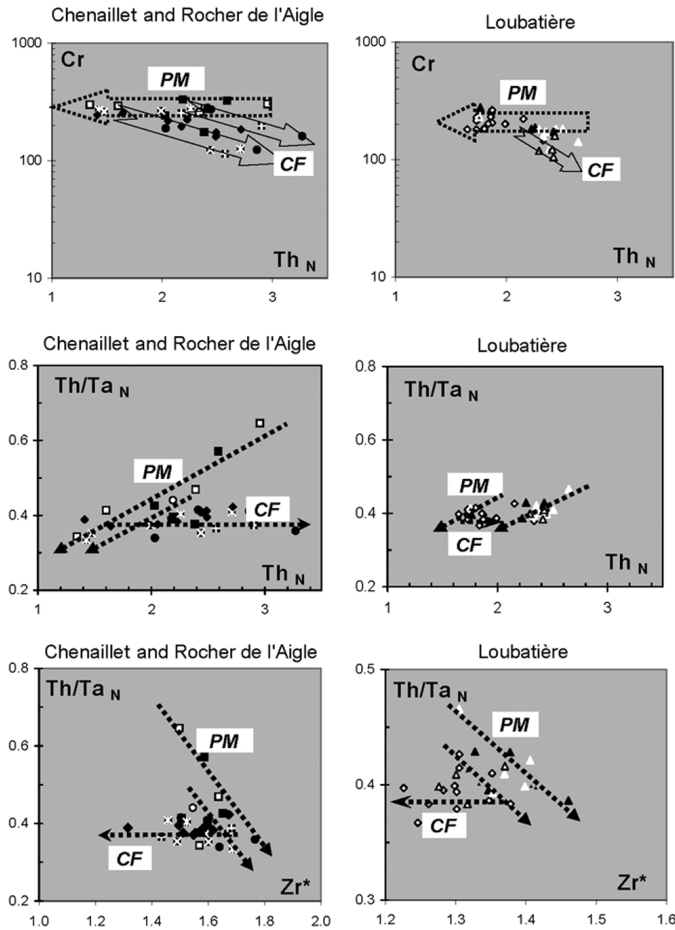


Figure 11. Correlations Cr versus Th_N and Th/Ta_N versus Th_N , which are evidence for partial melting (PM) and crystal fractionation (CF) relationships between sample lavas in each sampling area. Same legend for samples as in figure 7.

comb systems display teeth trending east-west, but many of them display teeth trending north-south (e.g., south flank of the Chenaillet massif, the northeastern extremity of the Loubatière; Fig. 1A and B), signifying that the surface enlargement during the building of the comb systems (three-quarters of the volcanic zone) occurred in two orthogonal directions, the main one being east-west.

That the stair systems predate the comb systems allows three consecutive stages of building of the abyssal hill to be distinguished: (1) mantle and gabbro exhumation alone; (2) uplift of the already exhumed basement synchronous with its rifting and the ascent of magma leading to the building of stair systems; and (3) the building of comb systems on a basement that was at once exhumed and uplifted during the eruptions. In such a situation, the deposition of fine-grained clastic sediments, reworking exclusively clasts of mantle and gabbro cataclasites, would have occurred locally on an already exhumed basement during the first and second stages. They would have been broken up and tilted during the third stage.

On the scale of the massif, the building of the five composite volcanoes (Fig. 1B), which correspond to the highest parts of relief, probably ended this last stage. In these composite structures, the exhumation operated along three or four fractures that radiated away from the center. As they link the narrow hummocky ridges between them, all the comb systems were probably built at the same time. On the whole, the main surface enlargement came from mantle exhumation along the three narrow ridges trending roughly north-south. The domed shape of the whole volcanic hill was probably created along with the building of the RA stair system. It was enhanced with the development, possibly along a transform fault, of three composite volcanoes (C, GC, and CS in Fig. 1B) aligned in an east-west direction in the middle of the eruptive area, synchronous with the building of comb systems with east-west branches on its southern flank.

In addition, the northeastern hill of mantle and gabbro, the crest of which is the prolongation of the volcanic crest southward, has probably been emplaced synchronously with the comb systems during the third stage. This northeastern basement zone was probably originally nonvolcanic. Indeed, the top of the mantle is either capped by cataclastic horizons or fractured and crosscut by calcite veinlets (ophicalcites 1 in Barféty et al., 1995) typical of mantle outcropping at the bottom of the sea (Tricart and Lemoine, 1989; Treves and Harper, 1994). On the western side of the massif, the mantle and the overlying exhumed gabbro sill, dotted with rare conic volcanoes and lower down the Chenaillet composite volcano, must have been emplaced before the building of any comb system during the first and second stages. It is likely that the three stages occurred one after the other without any interruption.

From my model (Fig. 14), it follows that at a slow spreading mid-ocean ridge, the basement is crosscut by a network of numerous deep high-angle (at shallow depth at least) detachment faults at the axial zone. Along these faults, serpentinized mantle peridotites, sometimes associated with thin gabbro bodies, are exhumed permanently. Basaltic magma could ascend up to the surface in some areas, forming abyssal hills. A volcanic hill would thus correspond to a short-wavelength segment, as defined by Murton and Parson (1993). In addition, the network of detachment faults is active along the axial zone only over some kilometers in total width, until it is relieved by normal faults for the transfer of material on the rift shoulders and replaced by another network of detachment faults at the axial ridge. Detachment faults are ephemeral, as is also inferred for the magma reservoirs. As underlined by Durand et al. (1996, p. 290 and references therein), "the detachment faults cannot be interpreted as long-lived structures, but instead may be thought of as transient in space, time and orientation." Furthermore, as eruptions of rather primitive magma are dominant, the feeder-dikes and thus the detachment faults along which mantle exhumation occurred must have been rooted close to or even in the mantle source.

Thus a close link must exist between lithospheric stresses,

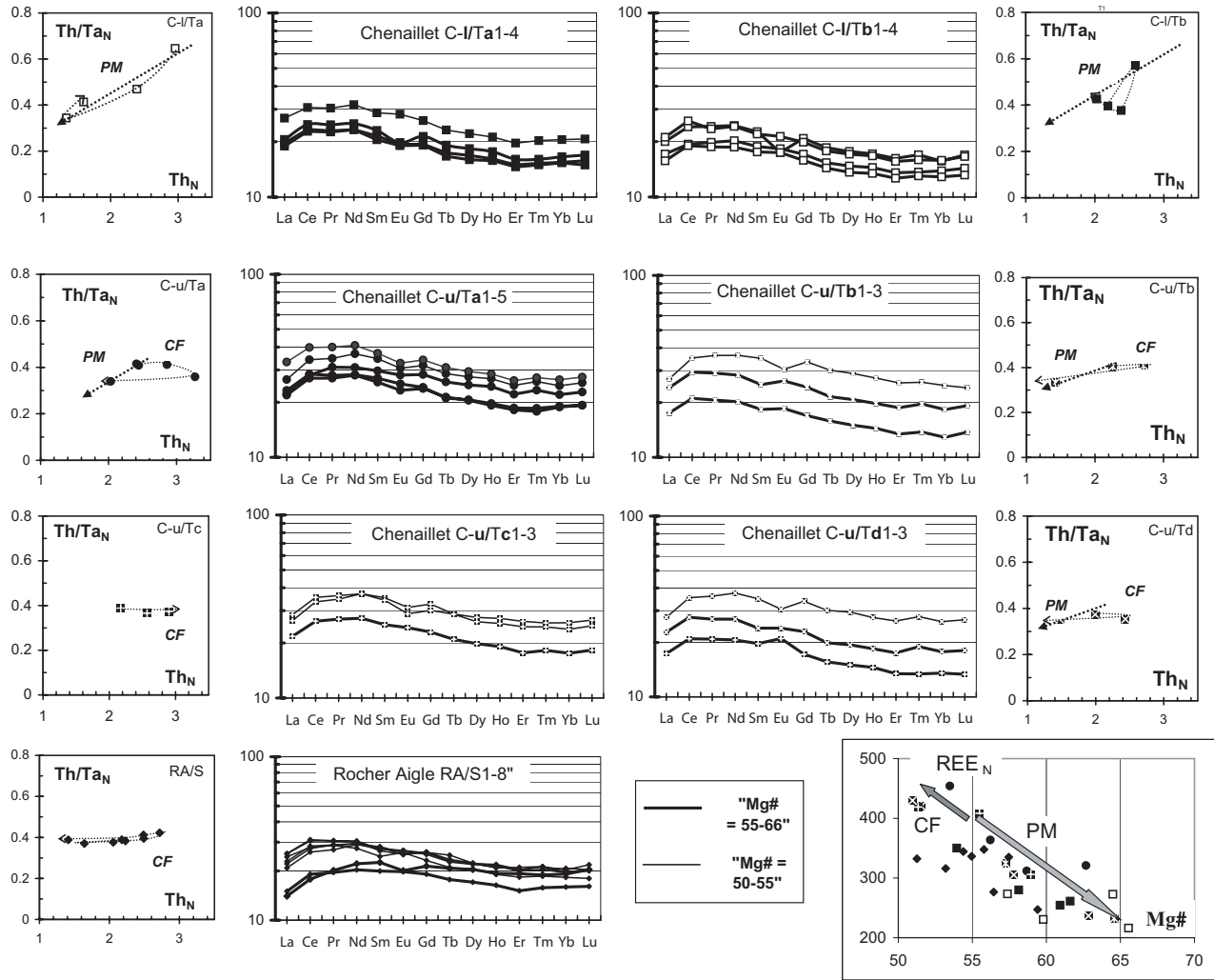


Figure 12. Chronology of eruptions (thinnest dotted line), partial melting (*PM* along the dotted line), and crystal fractionation (*CF*) relationships, visualized by correlation of Th/Ta_N versus Th_N on the one hand, and on the other, the evolution of $Mg\#$ with the Ch-normalized rare earth element (REE) abundance patterns and the sum of REE_N . Same legend for samples as in Figure 7.

which enable both mantle exhumation and formation of transient fractures up to the surface, and asthenospheric mantle melting. As specified by Green (2000), asthenospheric upwelling below the axial zone is a consequence of lithospheric plate motion, and not vice versa (i.e., plate motion is not a consequence of asthenospheric upwelling) (Murton and Parson, 1993). Such a model fits with the large-scale structure of a mid-ocean ridge and the mechanisms proposed by Doglioni (1990, 2003) to explain oceanic spreading.

It follows that melting is triggered by adiabatic decompression of the upper part of the asthenosphere below the mantle lithosphere in a process of upward and lateral transfer at the boundary between both divergent plates. The conditions of decoupling (and possibly also shearing) between the mantle asthenosphere and lithosphere at the plate boundaries may or may not trigger mantle melting. If magma is generated, which

is usually the case, the stress conditions of the mantle lithosphere would determine whether transient fractures could form extending up to the surface, giving birth to volcanoes. If not, intrusive thin gabbro bodies would form. A number of these gabbros are subsequently exhumed along with their host mantle.

CONCLUSIONS

This study of the Chenaillet ophiolite combines field data on volcano architectures and their mantle and gabbro basement, the relative chronology of eruptions, and geochemical data from the lavas. It demonstrates that this ophiolite can be considered to be a preserved portion of the axial volcanic ridge of an upper Jurassic slow spreading ocean similar to the MAR. The paleo-overthrust has been preserved and, except for erosion effects, the present topography corresponds to a structural surface close to

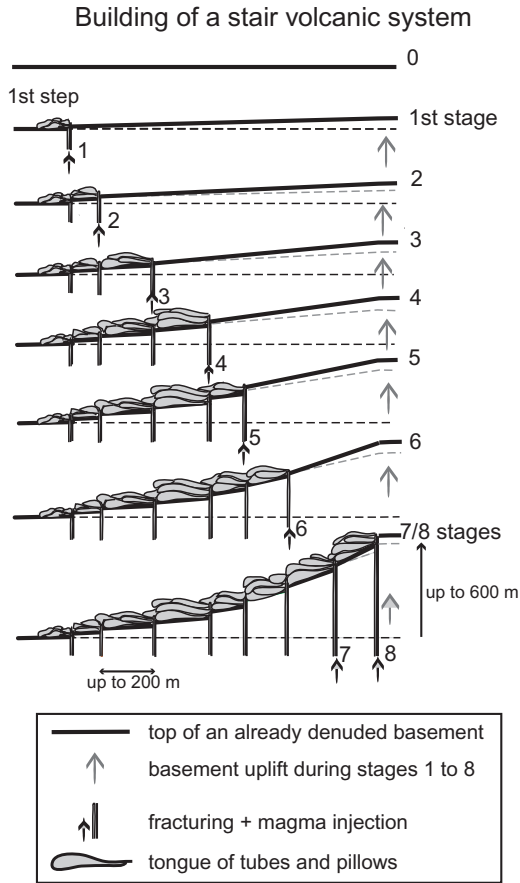


Figure 13. Two-dimensional model proposed for the building of a stair system.

the original topography. This 30-km² portion includes an abyssal hill 18 km² in area, with its nonvolcanic surroundings.

In the abyssal hill, the geometry of single volcanoes and the organization of volcanoes between them reveal two fundamentally distinct models of lava emplacement on the sea floor: (1) pillow tongues emplaced on the steps of a stair system; and (2) pillow conic volcanoes or hummocks, with dikes in their center, aligned on parallel teeth that are oblique to the branch of the comb system. In both systems volcanoes are emplaced on basement slopes much steeper in the comb system. The higher the edifice, the younger it is relative to the others. Each volcanic system represents one eruptive cycle and affects only a small area (stair, ≤ 1 km²; comb, 0.01–0.1 km²).

The comb systems postdate the stair systems and are the most numerous. They are often aligned and form in echelon chains along the crests of the ridges, taking on the appearance of hummocky ridges. Where they are associated, they form triple junctions where large composite volcanoes form.

These varied architectures reveal the reduced thickness of the basaltic crust (≤ 50 m now, but possibly ≤ 100 m before erosion). The volcanic relief of the abyssal hill is due to the accentuated undulations of the top of the underlying serpentinized

mantle basement. Up to now, this result concerning the origin of the volcanic relief at present axial zones could only be deciphered using gravity and/or seismic data in present oceans, leading to a preferred model involving a much thicker crust.

In other ways, the different geometries of the volcanic systems arise because the stair systems postdated basement exhumation, whereas comb systems were coeval with that exhumation.

The stair system was built by uplift, step-by-step fracturing of an already exhumed basement, and by magma injection along fissures that formed successively from the base to the top of the stair. In the comb system, volcanoes formed in line on the crest of a basement in uplift, at the intersection between a steeply dipping major fracture serving as feeder-dike and a set of shallow secondary fractures. Once formed, volcanoes were repeatedly transported away and downward to make room for a new line of volcanoes, such that the magma reservoir remained located below the crest of the ridge in formation. They traveled on new exhumed basement (mantle or gabbro), the top of which was underlain by an active detachment fault. At depth, this detachment fault superimposed on the wall of the major fracture. The small sizes of the comb systems suggest that the surface enlargement at the axial zone resulted in the activity of numerous short-lived detachment faults.

In each system, the small erupted lava volume, the very low crystallization rate of lavas, and the compositional variations in time suggest the existence of a small, periodically replenished and tapped magma chamber. The compositional variations differ slightly from one system to another, suggesting the activity of multiple magma chambers beneath the abyssal hill. Trace element correlations suggest that the erupted magmas are often related by partial melting relationships, which implies that feeder-dikes were rooted close to or even in the mantle source.

Thus a close link must exist between lithospheric stresses, enabling both mantle exhumation and formation of transient fractures up to the surface, and asthenospheric mantle melting. This process could be induced by adiabatic decompression (and possibly shearing) of the upper part of the asthenosphere below the mantle lithosphere during the process of upward and lateral transfer at the boundaries between both divergent plates. It did not result from upward convection from great depth in the asthenosphere. The plate tectonic model proposed by Doglioni (2003) supports such a hypothesis.

ACKNOWLEDGMENTS

This study was supported by the project "Relationships between magmatism and deformation during the transition of rifting to sea floor spreading," funded by the Research Group on Margins and the Bureau de Recherches Géologiques et Minières (Orléans). I thank P. Huchon (Paris VI University) and P. Rossi (BRGM) for their confidence and financial support. I sincerely acknowledge the reviewers J. Shervais, J. Natland, D. Presnall, and D. Anderson for their numerous helpful and constructive remarks and comments on this study, and G. Foulger for having greatly

Formation of volcanoes within a comb-type system

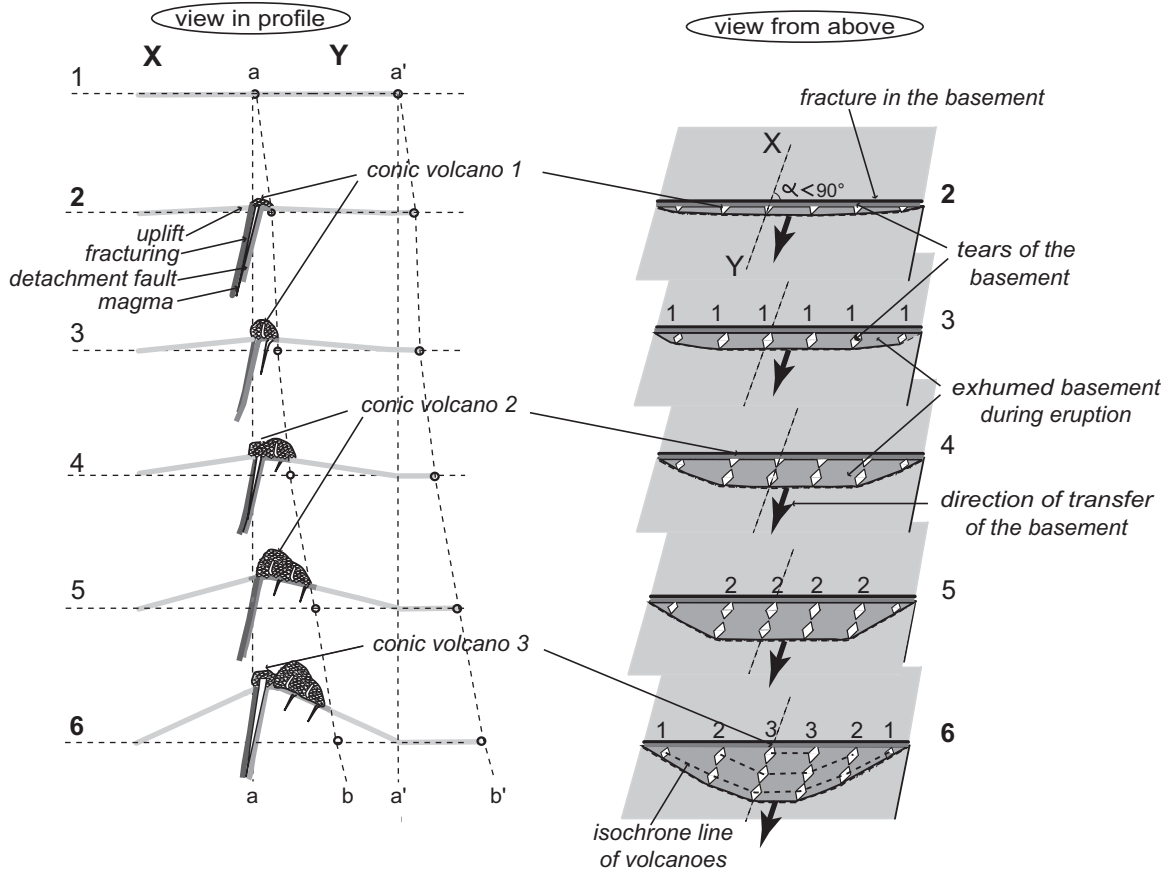


Figure 14. Three-dimensional model proposed for the building of a comb system. Stages 1–6 show the successive emplacement, in profile and from above, of three conic volcanoes with basement uplift, its fracturing, and the formation of a detachment fault concurrent with the ascent of magma. The sea floor enlargement is visualized with a progressively higher gap between marks a and b, a' and b'. See text for more detailed explanation.

improved the English of this paper during the reviewing process and for her pertinent and always constructive comments. This is contribution 1716 of the CRPG-CNRS.

REFERENCES CITED

- Allerton, S., Murton, B.J., Searle, R.C., and Jones, M., 1995, Extensional faulting and segmentation of the Mid-Atlantic Ridge north of the Kane Fracture Zone: *Marine Geophysical Research*, v. 17, p. 37–61.
- Allerton, S., Searle, R.C., and Murton, B.J., 1996, Bathymetric segmentation and faulting on the Mid-Atlantic Ridge, 24°00'N to 24°40'N, in McLeod, C.J., et al., eds., *Tectonic, magmatic, hydrothermal and biological segmentation of Mid-Ocean ridges*: Geological Society of London Special Publication 118, p. 49–60.
- Appelgate, B., and Shor, A., 1994, The northern Mid-Atlantic and Reykjanes ridges: Spreading center morphology between 55°50'N and 63°00'N: *Journal of Geophysical Research*, v. 99, B9, p. 17,935–17,956, doi: 10.1029/93JB03459.
- Auzende, J.M., Tivey, M., Cannat, M., Gente, P., Henriot, J.P., Juteau, T., Karson, J., and Lagabrielle, Y., 1993, Première exploration in situ de la dorsale médio-Atlantique au sud de la zone de fracture Atlantis (29°06'N–43°11'W): *Comptes Rendu Académie Sciences Paris, série II*, v. 316, p. 1415–1422.
- Ballard, R.D., and van Andel, T.H., 1977, Morphology and tectonics of the inner rift valley at lat 36°50'N on the Mid-Atlantic Ridge: *Geological Society of America Bulletin*, v. 88, p. 507–530.
- Barfély, J.C., Lemoine, M., de Gracianski, P.C., Tricart, P., Mercier, D., in collaboration with de Pêcher, A., Bertrand, J., Nievergelt, P., Amaudric du Chaffaut, S., Dumont, T., Monjuvent, G., Goffé, B., Kienast, J.R., Mevel, C., Gravost, M., Sauret, B., Godefroy, P., and Martin, C., 1995, Notice explicative, Carte géologique de France (1/50,000), feuille Briançon (823): Orléans, France, BRGM, 180 p. (in French).
- Barfély, J.C., Lemoine, M., Mercier, D., Polino, R., Nievergelt, P., Bertrand, J., Dumont, T., Amaudric du Chaffaut, S., Pêcher, A., and Monjuvent, G., 1996, Carte géologique de France (1/50,000), feuille Briançon (823): Orléans, BRGM (in French).
- Batiza, R., and Vanko, D., 1983, Volcanic development of small oceanic central volcanoes on the flanks of the East Pacific Rise inferred from narrow-beam echo-sounder surveys: *Marine Geology*, v. 54, p. 53–90, doi: 10.1016/0025-3227(83)90008-7.
- Bertrand, J., Courtin, B., and Vuagnat, M., 1981, Le massif ophiolitique du

- Montgenèvre Hautes Alpes, France, et province de Turin, Italie: Données nouvelles sur un vestige de manteau supérieur et de croûte océanique liguro-piémontais: *Bulletin Suisse Mineralogie Pétrographie*, v. 61, p. 305–322 (in French).
- Bertrand, J., Courtin, B., and Vuagnat, M., 1982, Elaboration d'un secteur de lithosphère océanique Liguro-Piémontais d'après l'ophiolite de Montgenèvre (Hautes-Alpes, France et province de Turin, Italie): *Ophioliti*, v. 2/3, p. 155–196 (in French).
- Bertrand, J., Nievergelt, P., and Vuagnat, M., 1985, Interpretation paléo-océanique d'une série pélagique à matériel ophiolitique: La Série de Chabrières, complexe de base du massif ophiolitique de Montgenèvre (Alpes Occidentales): *Comptes Rendu Académie Sciences Paris, série II*, v. 301, p. 16 (in French).
- Bertrand, J., Dietrich, V., Nievergelt, P., and Vuagnat, M., 1987, Comparative major and trace element geochemistry of gabbroic and volcanic rock sequences, Mongenèvre ophiolite, western Alps: *Schweizerische Mineralogische und Petrographische Mitteilungen*, v. 67, p. 147–169.
- Caby, R., 1995, Plastic deformation of gabbros in a slow-spreading Mesozoic ridge: Example of the Mongenèvre Ophiolite, western Alps, in *Visser, R.L.M., and Nicolas, A., eds., Mantle and lower crust exposed in oceanic ridges and in ophiolites: Norwell, Massachusetts, Kluwer Academic*, p. 123–145.
- Cannat, M., 1993, Emplacement of mantle rocks in the seafloor at mid-ocean ridges: *Journal of Geophysical Research*, v. 98, B3, p. 4163–4172.
- Cannat, M., 1996, How thick is the magmatic crust at slow spreading ocean ridges?: *Journal of Geophysical Research*, v. 98, p. 4163–4172.
- Cannat, M., and Casey, J.F., 1995, An ultramafic lift at the Mid-Atlantic Ridge: Successive stages of magmatism in serpentinized peridotites from the 15°N region, in *Visser, R.L.M., and Nicolas, A., eds., Mantle and lower crust exposed in oceanic ridges and in ophiolites: Norwell, Massachusetts, Kluwer Academic*, p. 5–34.
- Cannat, M., Lagabriele, Y., Bougault, H., Casey, J., de Coutures, N., Dmitriev, L., and Fouquet, Y., 1997, Ultramafic and gabbroic exposures at the Mid-Atlantic Ridge: Geological mapping in the 15°N region: *Tectonophysics*, v. 279, p. 193–213, doi: 10.1016/S0040-1951(97)00113-3.
- Cannat, M., Rommevaux-Jestin, C., Sauter, D., Deplus, C., and Mendel, V., 1999, Formation of the axial relief at the very slow spreading southwest Indian ridge (49° to 69°E): *Journal of Geophysical Research*, v. 104, B10, p. 22,825–22,843, doi: 10.1029/1999JB900195.
- Caroff, M., 1995, Open system crystallization and mixing in two layer magma chambers: *Lithos*, v. 36, p. 85–102, doi: 10.1016/0024-4937(95)00008-4.
- Caroff, M., Maury, R.C., Guille, G., and Cotton, J., 1997, Partial melting below Tubuai (Austral Islands, French Polynesia): *Contributions to Mineralogy and Petrology*, v. 127, p. 369–382, doi: 10.1007/s004100050286.
- Casey, J.F., 1997, Comparison of major- and trace-element geochemistry of abyssal peridotites and mafic plutonic rocks with basalts from the MARK region of Mid-Atlantic Ridge, in *Proceedings of the Ocean Drilling Program, scientific results*, v. 153: College Station, Texas, Ocean Drilling Program, p. 181–241.
- Chalot-Prat, F., Ganne, J., and Lombard, A., 2003, No significant element transfer from the oceanic plate to the mantle wedge during subduction and exhumation of the Tethys Ocean (western Alps): *Lithos*, v. 69, p. 69–103, doi: 10.1016/S0024-4937(03)00047-1.
- Chalot-Prat, F., Coco, E., and Bourlier, P.-Y., 2005, L'ophiolite du Chenaillet (Montgenèvre, Alpes franco-italiennes), témoin d'un segment de ride volcanique axiale d'un océan à croissance lente: *Géologie de la France*, in press (in French).
- Costa, S., and Caby, R., 2001, Evolution of the Ligurian Tethys in the western Alps: Sm/Nd and U/Pb geochronology and rare earth element geochemistry of the Montgenèvre Ophiolite (France): *Chemical Geology*, v. 175, p. 449–466, doi: 10.1016/S0009-2541(00)00334-X.
- Crane, K., and Ballard, R.D., 1981, Volcanics and structure of the Famous Narrowgate rift: Evidence for cyclic evolution: *Journal of Geophysical Research*, v. 86, B6, p. 5112–5124.
- Dauteuil, O., and Brun, J.-P., 1993, Oblique rifting in a slow spreading ridge: *Nature*, v. 361, p. 145, doi: 10.1038/361145a0.
- Desmurs, L., Müntener, O., and Manatschal, G., 2002, Onset of magmatic accretion within a magma-poor rifted margin: A case study from the Platta ocean-continent transition, eastern Switzerland: *Contributions to Mineralogy and Petrology*, v. 144, p. 365–382.
- Dick, H.J.B., 1989, Abyssal peridotites, very slow spreading ridges and ocean ridge magmatism, in *Saunders, A.D., and Norry, M.J., eds., Magmatism in the ocean basins: London, Geological Society of London Special Publication 42*, p. 71–105.
- Dogliani, C., 1990, The global tectonic pattern: *Journal of Geodynamics*, v. 12, p. 21–38, doi: 10.1016/0264-3707(90)90022-M.
- Dogliani, C., 2003, Rift asymmetry and continental uplift: *Tectonics*, v. 22, p. 1–13.
- Durand, C., Gente, P., and Dauteuil, O., 1995, Caractéristiques morphologiques des segments axiaux de la dorsale Médio-Atlantique entre 20°N et 24°N. *Comptes Rendu Académie Sciences Paris, série IIa*, v. 320, p. 411–418 (in French).
- Durand, C., Ballu, V., Gente, P., and Dubois, J., 1996, Horst and graben structures on the flanks of the Mid-Atlantic Ridge in the MARK area (23°22'N): Submersible observations: *Tectonophysics*, v. 265, p. 275–297, doi: 10.1016/S0040-1951(96)00049-2.
- Fudral, S., 1998, Etude géologique de la suture téthysienne dans les Alpes franco-italiennes nord-occidentales de la doire Ripaire (Italie) à la région de Bourg-Saint-Maurice (France): *Grenoble, Mémoire Géologie Alpine 29*, 2 vols. (in French).
- Gente, P., Mével, C., Auzende, J.M., Karson, J.A., and Fouquet, Y., 1991, An example of a recent accretion on the Mid-Atlantic Ridge: The Snake pit neovolcanic ridge (MARK area, 23°22'N): *Tectonophysics*, v. 190, p. 1–29, doi: 10.1016/0040-1951(91)90352-S.
- Green, D.H., 2000, Magmatism originating in the upper mantle, in *Proceedings of the International School, Earth and Planetary Sciences, crust-mantle interactions*, Siena, 2000, p. 77–95.
- Green, D.H., 2001, Primary magmas and mantle temperatures: *European Journal of Mineralogy*, v. 13, p. 437–451, doi: 10.1127/0935-1221/2001/0013-0437.
- Gudmundsson, A., 1995, Stress fields associated with oceanic transform faults: *Earth and Planetary Science Letters*, v. 136, p. 603–614, doi: 10.1016/0012-821X(95)00164-8.
- Head, J.W., III, Wilson, L., and Smith, D.K., 1996, Mid-ocean ridge eruptive vent morphology and substructure: Evidence for dike widths, eruption rates, and evolution of eruptions and axial volcanic ridges: *Journal of Geophysical Research*, v. 101, B12, p. 28,265–28,280, doi: 10.1029/96JB02275.
- Juteau, T., and Maury, R., 1999, *Géologie de la croûte océanique: Pétrologie et dynamique endogène*: Paris, Dunod, 367 p. (in French).
- Karson, J.A., Thompson, G., Humpris, S.E., Edmond, J.M., Bryan, W.B., Brown, J.R., Winters, A.T., Pockalny, R.A., Casey, J.F., Cambell, C., Klinkhammer, G., Palmer, M.R., Kinzler, R.J., and Sulanowska, M., 1987, Along axis variations in seafloor spreading in the MARK area: *Nature*, v. 328, p. 681–685, doi: 10.1038/328681a0.
- Kempton, P.D., and Casey, J.F., 1997, Petrology and geochemistry of cross-cutting diabase dikes, sites 920 and 921, in *Proceedings of the Ocean Drilling Project, scientific results*, v. 153: College Station, Texas, Ocean Drilling Program, p. 363–377.
- Kuo, B.-Y., and Forsyth, D.W., 1988, Gravity anomalies of the ridge-transform system in the south Atlantic between 31 and 34.5°S: Upwelling centers and variations in crustal thickness: *Marine Geophysical Research*, v. 10, p. 205–232, doi: 10.1007/BF00310065.
- Lagabriele, Y., 1987, Les ophiolites: Marqueurs de l'histoire tectonique des domaines océaniques: Le cas des Alpes franco-italiennes (Queyras, Piémont); comparaison avec les ophiolites d'Antalya (Turquie) et du Coast Range de Californie [Ph.D. thesis]: Brest, France, University of Bretagne Occidentale, 349 p. (in French).

- Lagabrielle, Y., 1994, Ophiolites of the southwestern Alps and the structure of the Tethyan oceanic lithosphere: *Ophioliti*, v. 19, p. 413–434.
- Lagabrielle, Y., and Cannat, M., 1990, Alpine Jurassic ophiolites resemble the modern central Atlantic basement: *Geology*, v. 18, p. 319–322, doi: 10.1130/0091-7613(1990)018<0319:AJORTM>2.3.CO;2.
- Lagabrielle, Y., and Lemoine, M., 1997, Alpine, Corsican and Apennine ophiolites: The slow-spreading ridge model: *Comptes Rendu Académie Sciences Paris, série II*, v. 325, p. 909–920.
- Lagabrielle, Y., Lemoine, M., and Tricart, P., 1985, Paléotectonique océanique et déformation alpines dans le massif ophiolitique du Pelvas d'Abriès (Alpes Occidentales–Queyras–France): *Bulletin de la Société Géologique de France*, v. 8, p. 4473–4479 (in French).
- Lagabrielle, Y., Bideau, D., Cannat, M., Karson, J.A., and Mevel, C., 1998, Ultramafic-mafic plutonic rock suites exposed along the Mid-Atlantic Ridge (10°N–30°N): Symmetrical-asymmetrical distribution and implications for seafloor spreading processes, in Buck, W.R., Delaney, P.T., Harrison, J.A., and Lagabrielle, Y., eds., *Faulting and Magmatism at Mid-Ocean Ridges*: Washington, D.C., American Geophysical Union Geophysical Monograph 106, p. 153–176.
- Lawson, K., Searle, R.C., Pearce, J.A., Browning, P., and Kempton, P., 1996, Detailed volcanic geology of the Marnok area, Mid-Atlantic Ridge north of Kane transform, in McLeod, C.J., et al., eds., *Tectonic, magmatic, hydrothermal and biological segmentation of mid-ocean ridges*: Geological Society of London Special Publication 118, p. 61–102.
- Lemoine, M., Tricart, P., and Boillot, G., 1987, Ultramafic and gabbroic ocean floor of the Ligurian Tethys (Alps, Corsica, Apennines): In search of a genetic model: *Geology*, v. 15, p. 622–625, doi: 10.1130/0091-7613(1987)15<622:UAGOFO>2.0.CO;2.
- Le Roex, A.P., Frey, F.A., and Richardson, S.H., 1996, Petrogenesis of lavas from the AMAR Valley and Narrowgate region of the FAMOUS Valley, 36°–37° N on the Mid-Atlantic Ridge: *Contributions to Mineralogy and Petrology*, v. 124, p. 167–184, doi: 10.1007/s004100050183.
- Lin, J., Purdy, G.M., Schouten, H., Sempere, J.-C., and Zervas, C., 1990, Evidence from gravity data for focused magmatic accretion along the Mid-Atlantic Ridge: *Nature*, v. 344, p. 627–632, doi: 10.1038/344627a0.
- Macdonald, K.C., Fox, P.J., Alexander, R.T., Pockalny, R., and Gente, P., 1996, Volcanic growth faults and the origin of Pacific abyssal hills: *Nature*, v. 380, p. 125–129, doi: 10.1038/380125a0.
- Mével, C., Caby, R., and Kienast, J.-R., 1978, Amphibolite facies conditions in the oceanic crust: Example of amphibolitized flaser-gabbro and amphibolites from the Chenaillet ophiolite massif (Hautes-Alpes, France): *Earth and Planetary Science Letters*, v. 39, p. 98–108, doi: 10.1016/0012-821X(78)90146-2.
- Mével, C., Cannat, M., Gente, P., Marion, E., Auzende, J.-M., and Karson, J.A., 1991, Emplacement of deep crustal and mantle rocks on the west median valley wall of the MARK area (MAR, 23°N): *Tectonophysics*, v. 190, p. 31–53, doi: 10.1016/0040-1951(91)90353-T.
- Meyzen, C.M., Toplis, M.J., Humler, E., Ludden, J.N., and Mevel, C., 2003, A discontinuity in mantle composition beneath the southwest Indian ridge: *Nature*, v. 421, p. 731–733, doi: 10.1038/nature01424.
- Murton, B.J., and Parson, L.M., 1993, Segmentation, volcanism and deformation of oblique spreading centers: A quantitative study of the Reykjanes ridge: *Tectonophysics*, v. 222, p. 237–257, doi: 10.1016/0040-1951(93)90051-K.
- Ohara, Y., Stern, R.J., Ishii, T., Yurimoto, H., and Yamazaki, T., 2002, Peridotites from the Mariana trough: First look at the mantle beneath an active back-arc basin: *Contributions to Mineralogy and Petrology*, v. 143, p. 1–18.
- Ohara, Y., Fujioka, K., Ishii, T., and Yurimoto, H., 2003, Peridotites and gabbros from the Parece Vela back-arc basin: Unique tectonic window in an extinct back-arc spreading ridge: *Geochemistry, Geophysics, Geosystems*, v. 4, no. 7, p. 1–22.
- Parson, L.M., Murton, B.J., Searle, R.C., Booth, D., Evans, J., Field, P., Keeton, J., Laughton, A., McAllister, E., Millard, N., Redbourne, L., Rouse, I., Shor, A., Smith, D., Spencer, S., Summerhayes, C., and Walker, C., 1993, En echelon axial volcanic ridges at the Reykjanes Ridge: A life cycle of volcanism and tectonics: *Earth and Planetary Science Letters*, v. 117, p. 73–87, doi: 10.1016/0012-821X(93)90118-S.
- Pezard, P.A., Anderson, R.N., Ryan, W.B., Becker, K., Alt, J.C., and Gente, P., 1992, Accretion, structure and hydrology of intermediate spreading rate oceanic crust from drillhole experiments and sea floor observations: *Marine Geophysical Research*, v. 14, p. 93–123.
- Presnall, D.C., Gudfinnsson, G.H., and Walter, M.J., 2002, Generation of mid-ocean ridge basalts at pressures from 1 to 7 Gpa: *Geochimica et Cosmochimica Acta*, v. 66, p. 2073–2090, doi: 10.1016/S0016-7037(02)00890-6.
- Pyle, D.G., Christie, D.M., Mahoney, J.J., and Duncan, R.A., 1995, Geochemistry and geochronology of ancient southeast Indian and southwest Pacific seafloor: *Journal of Geophysical Research*, v. 100, p. 22,261–22,282, doi: 10.1029/95JB01424.
- Ramberg, I.B., and van Andel, T.H., 1977, Morphology and tectonic evolution of the rift valley at lat 36°30'N, Mid-Atlantic Ridge: *Geological Society of America Bulletin*, v. 88, p. 577–586.
- Rampone, E., and Piccardo, G.B., 2000, The ophiolite-oceanic lithosphere analogue: New insights from the northern Apennines (Italy), in Dilck, Y., et al., eds., *Ophiolites and oceanic crust: New insights from field studies and the Ocean Drilling Program*: Boulder, Colorado, Geological Society of America Special Paper 349, p. 21–34.
- Rampone, E., Hofmann, A.W., Piccardo, G.B., Vannucci, R., Bottazzi, P., and Ottolini, L., 1995, Petrology, mineral and isotope geochemistry of the External Liguride peridotites (northern Apennines, Italy): *Journal of Petrology*, v. 36, p. 81–105.
- Rampone, E., Hofmann, A.W., Piccardo, G.B., Vannucci, R., Bottazzi, P., and Ottolini, L., 1996, Trace element and isotope geochemistry of depleted peridotites from an N-MORB type ophiolite (Internal Ligurides, N. Italy): *Contributions to Mineralogy and Petrology*, v. 123, p. 61–76, doi: 10.1007/s004100050143.
- Rampone, E., Hofmann, A.W., and Raczek, I., 1998, Isotopic contrasts within the Internal Liguride ophiolite (N. Italy): The lack of a genetic mantle-crust link: *Earth and Planetary Science Letters*, v. 163, p. 175–189, doi: 10.1016/S0012-821X(98)00185-X.
- Searle, R., Cowie, P.A., Mitchell, N.C., Allerton, S., MacLeod, C.J., Escartin, J., Russell, S.M., Slootweg, P.A., and Tanaka, T., 1998a, Fault structure and detailed evolution of a slow spreading ridge segment: The Mid-Atlantic Ridge at 29°N: *Earth and Planetary Science Letters*, v. 154, p. 167–183, doi: 10.1016/S0012-821X(97)00160-X.
- Searle, R., Keeton, J.A., Owens, R.B., White, R.S., Mecklenburgh, R., Parsons, B., and Lee, S.M., 1998b, The Reykjanes ridge: Structure and tectonics of a hot-spot influenced, slow spreading ridge, from multibeam bathymetry, gravity and magnetic investigations: *Earth and Planetary Science Letters*, v. 160, p. 463–478, doi: 10.1016/S0012-821X(98)00104-6.
- Sempéré, J.-C., Purdy, G.M., and Schouten, H., 1990, Segmentation of the Mid-Atlantic Ridge between 24°N and 30°40'N: *Nature*, v. 344, p. 427–431, doi: 10.1038/344427a0.
- Smith, D.K., and Cann, J.R., 1990, Hundreds of small volcanoes on the median valley floor of the Mid-Atlantic Ridge at 24–30°N: *Nature*, v. 348, p. 152–155, doi: 10.1038/348152a0.
- Smith, D.K., and Cann, J.R., 1992, The role of seamount volcanism in crustal construction at the Mid-Atlantic Ridge (24°–30°N): *Journal of Geophysical Research*, v. 97, B2, p. 1645–1658.
- Smith, D.K., and Cann, J.R., 1993, Building the crust at the Mid-Atlantic Ridge: *Nature*, v. 365, p. 707–715, doi: 10.1038/365707a0.
- Smith, D.K., and Cann, J.R., 1999, Constructing the upper crust of the Mid-Atlantic Ridge: A reinterpretation based on the Puna ridge, Kilauea volcano: *Journal of Geophysical Research*, v. 104, B11, p. 25,379–25,399, doi: 10.1029/1999JB900177.
- Smith, D.K., Cann, J.R., Dougherty, M.E., Lin, J., Spencer, S., MacLeod, C., Keeton, J., McAllister, E., Brooks, B., Pascoe, R., and Robertson, W., 1995a,

- Mid-Atlantic Ridge volcanism from deep-towed side-scan sonar image, 25°–29°N: *Journal of Volcanology and Geothermal Research*, v. 67, p. 233–262, doi: 10.1016/0377-0273(94)00086-V.
- Smith, D.K., Humphris, S.E., and Bryan, W.B., 1995b, A comparison of volcanic edifices at the Reykjanes ridge and the Mid-Atlantic Ridge at 24°–30°N: *Journal of Geophysical Research*, v. 100, B11, p. 22,485–22,498, doi: 10.1029/95JB02392.
- Stakes, D.S., Shervais, J.W., and Hopson, C.A., 1984, The volcanic-tectonic cycle of the Famous and Amar valleys, Mid-Atlantic Ridge (36°47'N): Evidence from basalt glass and phenocryst compositional variations for a steady state magma chamber beneath the valley midsections, AMAR 3: *Journal of Geophysical Research*, v. 89, B8, p. 6995–7028.
- Treves, B.E., and Harper, G.D., 1994, Exposure of serpentinites on the ocean floor: Sequence of faulting and hydrofracturing in the northern Apennine ophiolites: *Ophioliti*, v. 14B, p. 435–466.
- Tricart, P., and Lemoine, M., 1989, The Queyras ophiolite west of Mont Viso (Western alps): Indicator of a peculiar ocean floor in the Mesozoic Tethys: *Journal of Geodynamics*, v. 13, p. 163–181, doi: 10.1016/0264-3707(91)90037-F.
- Tron, V., and Brun, J.-P., 1991, Experiments on oblique rifting in brittle-ductile systems: *Tectonophysics*, v. 188, p. 71–84, doi: 10.1016/0040-1951(91)90315-J.
- Whitmarsh, R.B., Manatschal, G., and Minshull, T.A., 2001, Evolution of magma-poor continental margins from rifting to seafloor spreading: *Nature*, v. 413, p. 150–154, doi: 10.1038/35093085.
- Zonenshain, L.P., Kuzmin, M.I., Lisitsin, A.P., Bogdanov, Y.A., and Baranov, B.V., 1989, Tectonics of the Mid-Atlantic rift valley between the TAG and MARK areas (26–24°N): Evidence for vertical tectonic: *Tectonophysics*, v. 159, p. 1–23, doi: 10.1016/0040-1951(89)90167-4.

MANUSCRIPT ACCEPTED BY THE SOCIETY JANUARY 3, 2005